SF 298 MASTER COPY KEEP THIS COPY FOR REPRODUCTION PURPOSES

REPORT DOCUMENTATION PAGE

Form Approved OMB NO. 0704-0188

1. AGENCY USE ONLY *(Leave blank)*	2. REPORT DATE	3. REPORT TYPE AND DATES COVERED
	20 February 1998	Final Progress Report 9/1/92-9/30/97

4. TITLE AND SUBTITLE

Analysis of Hydrogen Diffusion in $LiNbO_3$ and III-V Semiconductor Crystals

5. FUNDING NUMBERS

DAAL03-89-D-0002

6. AUTHOR(S)

H. C. Casey, Jr.

7. PERFORMING ORGANIZATION NAMES(S) AND ADDRESS(ES)

Department of Electrical and Computer Engineering
Box 90291
Duke University
Durham, NC 27708-0291

8. PERFORMING ORGANIZATION REPORT NUMBER

HCC98-2

9. SPONSORING / MONITORING AGENCY NAME(S) AND ADDRESS(ES)

U.S. Army Research Office
P.O. Box 12211
Research Triangle Park, NC 27709-2211

10. SPONSORING / MONITORING AGENCY REPORT NUMBER

ARO 30763.1-EL

11. SUPPLEMENTARY NOTES

The views, opinions and/or findings contained in this report are those of the author(s) and should not be construed as an official Department of the Army position, policy or decision, unless so designated by other documentation.

12a. DISTRIBUTION / AVAILABILITY STATEMENT

Approved for public release; distribution unlimited.

12 b. DISTRIBUTION CODE

13. ABSTRACT *(Maximum 200 words)*

The goal of this project was to investigate waveguiding in optoelectronic crystals. Studies of the correlation between hydrogen (H) concentration and the extraordinary refractive index n_e in proton-exchanged lithium niobate ($LiNbO_3$) were resolved by partitioning the total H into optically active substitutional H and optically inactive interstitutial H. These results were summarized in two publications: Aplied Physics Letters, **63**, 718 (1993) and Journal of Applied Physics, **77**, 2697 (1995). Studies were initiated on the group-III nitrides. These studies included the investigation of the surface properties of GaN, the absorption coefficient in GaN, and the emission properties of blue light-emitting diodes. The results on GaN were summarized in three publications: Applied Physics Letters **68**, 1850 (1996), Applied Physics Letters **68**, 2867 (1996), and Applied Physics Letters **71**, 2572 (1997).

14. SUBJECT TERMS

Hydrogen diffusivity in $LiNbO_3$, groupd-III nitride

15. NUMBER IF PAGES

16. PRICE CODE

17. SECURITY CLASSIFICATION OR REPORT	18. SECURITY CLASSIFICATION OF THIS PAGE	19. SECURITY CLASSIFICATION OF ABSTRACT	20. LIMITATION OF ABSTRACT
UNCLASSIFIED	UNCLASSIFIED	UNCLASSIFIED	UL

Correlation of substitutional hydrogen to refractive index profiles in annealed proton-exchanged Z- and X-cut $LiNbO_3$

J. M. Zavada

U. S. Army Research Office, Research Triangle Park, North Carolina 27709

H. C. Casey, Jr., and R. J. States

Department of Electrical Engineering, Duke University, Durham, North Carolina 27708-0291

S. W. Novak

Evans East, Inc., Plainsboro, New Jersey 08536

A. Loni

Defense Research Agency, Great Malvern, Worcestershire, WR14 3PS, United Kingdom

Abstract

Previous disagreements concerning a linear correlation between the hydrogen (H) concentration and the extraordinary refractive index n_e in proton-exchanged lithium niobate ($LiNbO_3$) have been resolved by partitioning the total H into optically active substitutional H and optically inactive interstitial H. The H and Li spatial variations in both Z-cut and X-cut crystals were determined by secondary-ion mass spectrometry (SIMS) with a quantitative evaluation in atoms/cm^3. These samples were proton exchanged in neat benzoic acid at 185°C and then were annealed at 400°C for times t from 6 to 240 min in wet flowing oxygen. For the Z-cut crystals, fit of the SIMS measured H profiles by expressions obtained from the diffusion equation for diffusion from a finite layer gave a substitutional H diffusivity of $D_s^Z = 5.0 \pm 0.3 \times 10^{-12}$ cm^2/s and an interstitial H diffusivity of $D_i^Z = 1.4 \pm 0.1 \times 10^{-11}$ cm^2/s. The wet flowing oxygen acts as a constant source of interstitial H at the surface with the diffusivity D_i^Z and gives an integrated H concentration due to the flowing wet oxygen which increases as $\sqrt{t}$. The Li diffusivity was $D_{Li}^Z = 4.8 \pm 0.2 \times 10^{-12}$ cm^2/s which is nearly equal to D_s^Z. For X-cut crystals, the substitutional H diffusivity was $D_s^X = 3.4 \pm 0.2 \times 10^{-12}$ cm^2/s and the interstitial diffusivity was $D_i^X = 1.3 \pm 0.2 \times 10^{-11}$ cm^2/s. The n_e profiles were evaluated by means of optical prism-coupling measurements and numerical simulations. In both cases of crystal orientation, the effective index diffusivity is nearly equal to the diffusivity of substitutional H. Furthermore, there is an excellent linear relationship between the n_e profile and the corresponding substitutional H distribution.

I. INTRODUCTION

Crystalline lithium niobate ($LiNbO_3$) is an important material for modern optoelectronic device applications. Due to its high electro-optic, acousto-optic, and non-linear optical coefficients, this material has found widespread use in optical modulation, optical switching, signal processing, and frequency conversion.[1] Proton-exchange (PE) of $LiNbO_3$ is an effective technique for formation of low loss, optical waveguides in this material. In this technique, hydrogen (H) atoms in the liquid melt are exchanged with Li atoms in the crystal which leads to a large increase in the extraordinary refractive index n_e.[2] However, annealing is typically required to eliminate compositional instabilities in the exchanged layer and to restore desirable optical properties such as the large electro-optic figure of merit.[3,4] In addition, the depth profile of n_e in the PE-$LiNbO_3$ layers is strongly dependent upon the annealing procedures.[5] Consequently, an understanding of the relationship between the redistribution of H atoms with annealing and the change in the refractive index is of particular importance in determining optimum device fabrication procedures.

Previously, we reported on the correlation of H depth concentrations with the extraordinary refractive index profiles in a set of annealed Z-cut PE-$LiNbO_3$ crystals.[6,7] The H distributions were determined by secondary ion mass spectrometry (SIMS) and optical characterization of the refractive index was done through laser prism-coupling techniques. It was found that the measured H concentration decreased more slowly with depth than a single Gaussian function, which is the appropriate solution to diffusion from a thin surface layer. However, the sum of the two separate Gaussians, one fit to the low H concentration region and another to the high H concentration region, yielded excellent agreement to the SIMS measured profiles.[8] In analogy with diffusion in semiconductors, the larger diffusivity was designated the interstitial coefficient D_i^Z and the smaller diffusivity,

the substitutional coefficient D_s^Z. It was possible to fit the effective index values for the observed modes with a single Gaussian and an index diffusivity D_n^Z was determined. The average value of D_n^Z was equal to the substitutional H diffusivity D_s^Z and the index depth profiles were in excellent linear agreement with the substitutional H distributions.[7] These results suggest that the change in the extraordinary refractive index depends on the substitutional H, which forms crystal bonds, rather than the total H concentration which includes interstitial H.

While partitioning of a diffusing species into substitutional and interstitial components is common in semiconductor materials, this concept has not been adequately addressed in the annealing of PE-$LiNbO_3$. However, there is experimental evidence that two H components are present in PE-$LiNbO_3$. Incorporation of H on substitutional lattice sites as well as on interstitial sites has been reported by Bollmann and Stöhr[9] and was based on absorption and electrical conductivity measurements. Magnetic resonance measurements by Engelsberg et al.[10] demonstrated the presence of both substitutional and interstitial H in annealed PE-$LiNbO_3$ crystals. Our diffusion analysis indicates a similar partitioning of H in annealed PE-$LiNbO_3$ and relates the substitutional component to changes in the refractive index.

In this paper, we extend our prior investigations to include both Z-cut and X-cut crystals and present a more rigorous model for analyzing H and Li diffusion in annealed PE $LiNbO_3$ crystals. For this model, the PE region represents an extended source for H diffusion into a semi-infinite region (substrate) and leads to a concentration profile which is the sum of two error functions.[11] The Li redistribution is similarly modeled as the Li diffusion from a semi-infinite source (substrate) into the PE region. Again, a composite function which is the sum of two error functions is obtained. While a single diffusivity leads to very good fits to the SIMS measured Li profiles, it is necessary to use two different diffusivities

to fit the H profiles. One is related to a slower-diffusing substitutional component and the other to a faster-diffusing interstitial component. Furthermore, we find that annealing PE-$LiNbO_3$ crystals in flowing wet oxygen produces an additional H source which needs to be included in the analysis. The refractive index profiles, that are determined by prism-coupling experiments, show excellent correlation with the substitutional H depth profiles in both Z-cut and X-cut samples.

Section II contains details of the experimental procedures used in this investigation, and the diffusion models for analysis of H, Li, and refractive index depth profiles are presented in Sec. III. In Sec. IV, the diffusion analysis is applied to the depth profiles found in annealed Z-cut PE-$LiNbO_3$ samples. The diffusion analysis for the depth profiles in annealed X-cut PE-$LiNbO_3$ samples is given in Sec. V. A summary of the present results is given in Sec. VI, including a discussion of similarities and differences found in the analysis of Z-cut and X-cut material. Questions concerning quantification standards in the SIMS measurements are also addressed.

II. EXPERIMENTAL PROCEDURES AND RESULTS

Two sets of $LiNbO_3$ crystals (Barr and Stroud) were used in this study, one Z-cut and the other X-cut. A proton-exchanged (PE) surface layer was produced in samples of each set by inserting the samples in a neat benzoic acid melt held at a temperature of 185°C for 70 min. The material and optical properties of the PE-$LiNbO_3$ samples were studied in their as-exchanged state and after furnace annealing. The samples were annealed in flowing wet oxygen (1.7 l/min) at 400°C for times ranging from 6 min to 240 min. Secondary ion mass spectrometry (SIMS) analysis was used to obtain quantitative H and Li depth distributions for these samples. Refractive index profiles in the exchanged samples were determined by optical waveguiding measurements.

A. Hydrogen and lithium depth profiles

Quantitative atomic depth profiles for H and Li in the as-exchanged and furnace annealed PE-$LiNbO_3$ samples were annalyzed using a Perkin-Elmer 6300 quadrupole-based instrument. The primary Cs ion beam energy was 8 keV and the impact angle was 60° measured from the normal. Lower impact energies at higher incidence angles have been shown to remove ion yield artifacts at the interface between the PE region and the bulk material.[12] With this method, there are no "bumps" in either the H or Li profiles at the PE-exchange interface. No conductive coating was applied prior to analysis. Profiles of H were acquired by monitoring negative atomic secondary ions whereas the Li profiles were obtained simultaneously by monitoring $CsLi^+$ molecular ions. Conversion of H ion count rates to concentrations was accomplished by using relative sensitivity factors calculated from analyses of a H ion-implanted $LiNbO_3$ standard which was measured during each analyitcal run. The H profiles were background subtracted using a background determined in the PE samples. The Li profiles were calibrated by setting the value of the profiles in the unexchanged region equal to the ideal atom density of Li in bulk $LiNbO_3$ (1.89×10^{22} atoms/cm^{-3}). Depth scales were calibrated by measuring the analytical crater depths with a stylus profilometer.

Figure 1 displays the H and Li depth profiles that were obtained for the Z-cut PE-$LiNbO_3$ crystals studied in this investigation. These samples were annealed in flowing wet oxygen at 400°C for times of 6, 15, 45, 90, 135, and 180 min. The H depth profiles that were obtained for the X-cut samples are shown in Fig. 2. The X-cut samples were annealed under the same conditions for 45, 120, and 240 min.

In the unannealed PE-$LiNbO_3$ samples, the H depth profiles consist of a plateau of constant H atom density, followed by a sharp decrease to the SIMS detection limit of about 5×10^{18} cm^{-3}.[11,13] For the present exchange conditions, the Z-cut samples have an exchange depth of 0.65 μm and a peak H concentration

of 6×10^{21} cm^{-3}. The X-cut samples have an exchange depth of 0.75 μm and a peak H concentration of 3.5×10^{21} cm^{-3}. While a step-like H profile is retained during the early stages of annealing, particularly at relatively low temperatures of approximately 275°C, annealing at higher temperatures of near 400°C rapidly produces a highly graded profile.[6] The graded H profile, with lower concentration, extends far deeper than the original exchange depth.

The behavior of the Li depth distributions is somewhat different than that of the H profiles. As a result of proton exchange, Li is depleted from the surface region of the $LiNbO_3$ crystal. The Li distribution in as-exchanged crystals is slightly graded at the surface and reaches the bulk substrate concentration of $C_{Li}^{bulk} = 1.89 \times 10^{22}$ cm^{-3} at a location that coincides with the depth of the PE plateau.[13] With annealing, Li from the substrate diffuses into the PE region and the Li profiles become increasingly shallow. Eventually, only a minor difference exists between the Li density near the surface and that in the substrate bulk.

B. Refractive index data

Previous investigations have indicated that the extraordinary refractive index n_e has an abrupt-step profile in unannealed PE-$LiNbO_3$ samples.[5,13] After annealing, this profile becomes highly graded. The data from the present experiments support such behavior for n_e. The PE-$LiNbO_3$ crystals were examined for optical waveguiding using a prism-coupling technique with a HeNe laser operating at $\lambda = 0.6328$ μm. Each as-exchanged sample was found to support a single TM guided mode, which is consistent with the exchange depth and a step-index change Δn_e^{PE} of approximately 0.10. After annealing, the samples were again characterized using a prism coupled laser. All of the annealed samples functioned as multimode waveguides and up to five modes in a single sample were observed. Effective index values N_e for the observed modes were calculated based on the prism-coupling parameters. An inverse WKB method[14] was used to determine

the $1/e$ depths d_{-1} of the modes for the samples that supported at least three propagating modes. Depths could not be associated with effective index values for as-exchanged samples and for samples with only two modes.

The optical waveguiding data for the Z-cut and X-cut samples are given in Table I and II, respectively. The effective index values N_e for the observed modes and the $1/e$ depths d_{-1} which were determined by the inverse WKB method are listed in these Tables.

III. DIFFUSION ANALYSIS FOR PE-$LiNbO_3$

A. Hydrogen diffusion

The diffusion of H from the PE layer is governed by the initial conditions of a thin surface layer with a constant amount of diffusant, as shown in Fig. 3 (a), and with no out diffusion of H from the crystal during annealing. Mathematically, the initial condition is expressed by:

$$C_H(x,0) = C_H^0 \qquad \text{for } 0 < x < \delta, \tag{1}$$

and

$$C_H(x,0) = 0 \qquad \text{for } x > \delta, \tag{2}$$

where C_H^0 is the initial H surface concentration after proton exchange. With the condition of zero H flow from the surface, the boundary condition is given by:

$$\left.\frac{\partial C_H(x,t)}{\partial x}\right|_{x=0} = 0, \tag{3}$$

where $C_H(x,t)$ is the H concentration in cm^{-3} at the distance x and time t. The resulting diffusion profiles are obtained by using the standard diffusion equation for diffusion from a finite layer into a semi-infinite body with a reflecting boundary at $x = 0$ and is given by:[15]

$$C_H(x,t) = \frac{C_H^0}{2}\left[\text{erf}\,\frac{(\delta + x)}{2\sqrt{Dt}} + \text{erf}\frac{(\delta - x)}{2\sqrt{Dt}}\right], \tag{4}$$

where erf is the error function, x is the distance in cm, D is the diffusivity in cm^2/s, t is the diffusion time in s, δ is the exchange depth in cm, and C_H^0 is the H surface concentration in cm^{-3} at $t = 0$.

When $\delta < \sqrt{Dt}$, Eq. (4) reduces to the Gaussian function:

$$\lim_{\delta \to 0} C_H(x,t) = \frac{Q_H^{PE}}{\sqrt{\pi Dt}} \exp(-x^2/4Dt), \tag{5}$$

where Q_H^{PE} is the amount of H per cm^2 in the PE layer and is given by:

$$Q_H^{PE} = C_H^0 \delta. \tag{6}$$

In a previous paper, a Gaussian function was used to analyze the H depth profiles in Z-cut annealed PE $LiNbO_3$.[8] When a single Gaussian function, as given in Eq. (5), was used to fit the H profiles, it was found that the measured H concentration decreased much more slowly than the Gaussian curve. At a depth of approximately 10δ, the calculated Gaussian curve was nearly an order of magnitude less than the measured profile.

In order to obtain a better fit, two separate Gaussian functions were fit to the experimental H profiles.[8] One Gaussian was fit to the low H concentration tail region and a second Gaussian was fit to the higher H concentration surface region so that the sum of the two Gaussians fit the measured profile. A diffusivity and surface concentration were obtained for each Gaussian function. The diffusivity obtained for the Gaussian, which was fit to the low H concentration substrate region, was designated the interstitial diffusivity D_i, and the diffusivity for the Gaussian which was fit to the high H concentration surface region was designated the substitutional diffusivity D_s. This approach led to very good fits for the experimental H data and indicated that two species of H are involved in the diffusion process.

When δ is approximately $\sqrt{Dt}$, it is more appropriate to use the erf representation given in Eq. (4) to analyze the H depth profiles. Figure 4 illustrates the

difference between using the error functions of Eq. (4) and two Gaussian functions as given by Eq. (5) to model the H depth profile for the Z-cut PE-$LiNbO_3$ crystals annealed for 6 and 45 min. It can be seen that while the overall differences are small, they are more significant at shorter annealing times.

As with the Gaussian function, use of a single equation of the form of Eq. (4) did not produce good fits to the experimental H data. Vohra et al.[11] previously tried using such an expression to fit H diffusion profiles. Their analysis also resulted in a calculated profile which decreased less rapidly in the low concentration tail region than the SIMS measured H profile. However, very good fits have been obtained to the data shown in Figs. 1 and 2 when two such expressions, with different diffusivities, were used.

Since the function which is given in Eq. (4) will occur often in this analysis, it is convenient to represent it as $F(x, \delta, Dt)$:

$$F(x, \delta, Dt) = \frac{1}{2}\left[\text{erf}\,\frac{(\delta + x)}{2\sqrt{Dt}} + \text{erf}\frac{(\delta - x)}{2\sqrt{Dt}}\right]. \tag{7}$$

The H concentration profile $C_H(x, t)$ is then given by:

$$C_H(x, t) = C_{H,s}^{PE} F(x, \delta, D_s t) + C_{H,i}^{PE} F(x, \delta, D_i t), \tag{8}$$

where $C_{H,s}^{PE}$ and $C_{H,i}^{PE}$ are the surface concentrations of the H diffusant in the substitutional and interstitial components, respectively. The sum of $C_{H,s}^{PE}$ and $C_{H,i}^{PE}$ is the total H concentration C_H^0 introduced into the crystal due to PE. The two diffusivities are D_s and D_i.

This approach implies that the total amount of H in the annealed PE-$LiNbO_3$ crystal remains constant. However, the experimental SIMS data indicated that the total amount of H actually increased with annealing time. This experimental result was found with both Z-cut and X-cut PE-$LiNbO_3$ samples. Since all samples were annealed in flowing wet oxygen, it appears that the flowing gas

collected water molecules and introduced H into the samples during annealing.[9] Consequently, another term was added to the H concentration profile $C_H(x,t)$ to account for this extra source of H. The flowing wet oxygen acts as a constant source of H at the surface:

$$C_H(0,t) = C_H^{wv} \qquad \text{for } t > 0, \tag{9}$$

and the solution of the diffusion equation from a constant source is the familiar:[16]

$$C_{H,i}^{wv}(x,t) = C_H^{wv}\text{erfc}\frac{x}{2\sqrt{D_i t}}, \tag{10}$$

where erfc is the complementary error function (1-erf). In Eq. (10), C_H^{wv} is the constant H surface concentration due to the water vapor. It is assumed that the H due to wet oxygen annealing enters the PE-$LiNbO_3$ samples primarily as an interstitial species. Therefore, the complete expression for the H concentration profile is:

$$C_H(x,t) = C_{H,s}^{PE}F(x,\delta,D_s t) + C_{H,i}^{PE}F(x,\delta,D_i t) + C_H^{wv}\text{erfc}\frac{x}{2\sqrt{D_i t}}. \tag{11}$$

This equation is the analytical expression that was used to model the H diffusion profiles in the annealed PE-$LiNbO_3$ samples. Two different diffusion mechanisms are represented: a finite layer diffusion source of the PE region and a constant surface diffusion source from the water vapor. This expression also involves two species of H, interstitial H and substitutional H, each having a different diffusivity. The interstitial H enters the samples from wet oxygen annealing as well as during PE. The substitutional H enters the crystal only through the PE.

The amount of H diffusant $Q_H(t)$ per cm^2 in the crystal after annealing for time t can be obtained by integrating Eq. (11) from $x = 0$ to $x = \infty$. There are three contributions to $Q_H(t)$, one from the substitutional H and the two from the interstitial H. Closed form expressions can be obtained for the integrals of the

new p. 11

collected water molecules and introduced H into the samples during annealing.[9] Consequently, another term was added to the H concentration profile $C_H(x,t)$ to account for this extra source of H. The flowing wet oxygen acts as a constant source of H at the surface:

$$C_H(0,t) = C_H^{wv} \qquad \text{for } t > 0, \tag{9}$$

and the solution of the diffusion equation from a constant source is the familiar:[16]

$$C_{H,i}^{wv}(x,t) = C_H^{wv}\text{erfc}\frac{x}{2\sqrt{D_i t}}, \tag{10}$$

where erfc is the complementary error function (1-erf). In Eq. (10), C_H^{wv} is the constant H surface concentration due to the water vapor. It is assumed that the H due to wet oxygen annealing enters the PE-$LiNbO_3$ samples primarily as an interstitial species. Therefore, the complete expression for the H concentration profile is:

$$C_H(x,t) = C_{H,s}^{PE}F(x,\delta,D_s t) + C_{H,i}^{PE}F(x,\delta,D_i t) + C_H^{wv}\text{erfc}\frac{x}{2\sqrt{D_i t}}. \tag{11}$$

This equation is the analytical expression that was used to model the H diffusion profiles in the annealed PE-$LiNbO_3$ samples. Two different diffusion mechanisms are represented: a finite layer diffusion source of the PE region and a constant surface diffusion source from the water vapor. This expression also involves two species of H, interstitial H and substitutional H, each having a different diffusivity. The interstitial H enters the samples from wet oxygen annealing as well as during PE. The substitutional H enters the crystal only through the PE.

The amount of H diffusant $Q_H(t)$ per cm^2 in the crystal after annealing for time t can be obtained by integrating Eq. (11) from $x = 0$ to $x = \infty$. There are three contributions to $Q_H(t)$, one from the substitutional H and the two from the interstitial H. Closed form expressions can be obtained for the integrals of the

error functions:

$$\int_0^\infty F(x,\delta,Dt)dx = \delta, \tag{12}$$

and

$$\int_0^\infty \mathrm{erfc}\frac{x}{2\sqrt{D_i t}}dx = 2\sqrt{\frac{D_i t}{\pi}}\ . \tag{13}$$

Equations (12) and (13) permit writing the time dependence of the total amount of H diffusant as:

$$Q_H(t) = Q_{H,s}^{PE} + Q_{H,i}^{PE} + C_H^{wv}\sqrt{4D_i t/\pi}. \tag{14}$$

According to this model, the total H diffusant increases with annealing time as the $\sqrt{t}$ due to the water vapor source. The H contribution from the proton-exchange remains constant.

B. Lithium diffusion

In order to analyze the Li profiles, the Li concentration in the as-exchanged sample was assumed to be a step function as represented in Fig. 3 (b), and that during annealing there is no outdiffusion of Li from the PE-$LiNbO_3$ crystals. Mathematically, the initial conditions are:

$$C_{Li}(x,0) = C_{Li}^0 \qquad \text{for } 0 < x < \delta, \tag{15}$$

and

$$C_{Li}(x,0) = C_{Li}^{bulk} \qquad \text{for } x > \delta, \tag{16}$$

where C_{Li}^0 is the Li surface concentration after PE, but before annealing, and C_{Li}^{bulk} is the Li concentration in bulk material. The boundary condition at the surface is:

$$\left.\frac{\partial C_{Li}(x,t)}{\partial x}\right|_{x=0} = 0, \tag{17}$$

where $C_{Li}(x,t)$ is the Li concentration profile after annealing for time t. These conditions represent diffusion from a semi-infinite extended source in the substrate for $x > \delta$ into a surface region from $0 < x < \delta$ with a reflecting boundary at

$x = 0$. During annealing, there is a concentration gradient which results in the Li diffusion. The solution to the diffusion equation for these conditions is the sum of two complementary error functions.[11,17] Simulation of the Li diffusion profiles with the use of *Mathematica*™ to rapidly compare calculated Li profiles with the SIMS measured Li profiles showed that the Li surface concentration could be taken as zero rather than as the measured value of $C_{Li}^{0} = 0.5 \times 10^{22}$ cm^{-3}. This simplification permits representing the Li diffusion profile as,

$$C_{Li}(x,t) = \frac{C_{Li}^{bulk}}{2}\left[\text{erfc}\,\frac{(\delta + x)}{2\sqrt{D_{Li}t}} + \text{erfc}\frac{(\delta - x)}{2\sqrt{D_{Li}t}}\right], \tag{18}$$

where D_{Li} is the Li diffusivity. With Eq. (18), good fits to the SIMS measured Li profiles for the annealed PE-$LiNbO_3$ samples were obtained. A single value for the Li diffusivity D_{Li} was sufficient for fitting the experimental curves and annealing in water vapor did not lead to an additional term.

C. Refractive index depth profiles

Several studies have shown that the extraordinary refractive index depth profile in as-exchanged PE-$LiNbO_3$ is approximately a step function.[5,13,18] With annealing, the index depth profile becomes highly graded. While these studies are based on indirect experimental techniques, it appears as if the refractive index were a physical quantity undergoing a diffusion process with annealing. Actually, the change in the index profile is a consequence of the H and Li diffusion. Nevertheless, it is possible to model the diffusion of the refractive index when annealed with the following initial conditions:

$$n_e(x,0) = n_e^{PE} \qquad \text{for } 0 < x < \delta, \tag{19}$$

and

$$n_e(x,0) = n_e^{bulk} \qquad \text{for } x > \delta. \tag{20}$$

The boundary condition at the surface is:

$$\left.\frac{\partial n_e(x,t)}{\partial x}\right|_{x=0} = 0. \tag{21}$$

Here, n_e^{bulk} is the extraordinary refractive index of the unchanged bulk crystal and n_e^{PE} is the index of the PE layer. The resulting solution to the diffusion equation for these conditions is:[15,19]

$$n_e(x,t) = n_e^{bulk} + \frac{\Delta n_e^{PE}}{2}\left[\text{erf}\,\frac{(\delta+x)}{2\sqrt{D_n t}} + \text{erf}\frac{(\delta-x)}{2\sqrt{D_n t}}\right], \tag{22}$$

where $\Delta n_e^{PE} = (n_e^{PE} - n_e^{bulk})$ is the initial index change for the as-exchanged crystal, and D_n is the index diffusivity.

As with the Li concentrations, it is possible to model the depth profile of the extraordinary refractive index in annealed PE-$LiNbO_3$ by the above expression with a single diffusivity D_n. No additional source terms were required due to annealing in water vapor. The total index diffusant Q_n can be found by integrating $[n_e(x,t) - n_e^{bulk}]$ from $x = 0$ to $x = \infty$. Integration of Eq. (22) gives:

$$Q_n = (n_e^{PE} - n_e^{bulk})\delta. \tag{23}$$

This quantity depends only on the PE conditions and should remain constant with annealing.

IV. ANALYSIS OF DATA FOR Z-CUT PE-$LiNbO_3$

A. Hydrogen depth profiles

The H depth profiles shown in Figs. 1 and 2 were analyzed using the composite expression for the H concentration $C_H(x,t)$ given in Eq. (11) . Since the following discussion refers to Z-cut material, we have added superscripts to the various quantities:

$$C_H^Z(x,t) = C_{H,s}^{Z-PE}F(x,\delta^Z,D_s^Z t) + C_{H,i}^{Z-PE}F(x,\delta^Z,D_i^Z t) + C_H^{Z-wv}\text{erfc}\frac{x}{2\sqrt{D_i^Z t}}. \tag{24}$$

As mentioned previously, this expression for the H concentration involves two different diffusivities and two different source terms. Two different diffusivities were required since good fits to the H depth profiles could not be obtained with a single diffusion coefficient. An example of this situation is shown in Fig. 5 where the H concentration represented by the single Gaussian of Eq. (5) is nearly an order of magnitude lower than the measured profile at a depth of $10\delta^Z$. The need for two different H source terms arises from the experimental SIMS data in which the total H in the crystal increases with annealing time in flowing wet oxygen. Consequently, a constant surface source term due to the water vapor had to be used in addition to the extended H source from the PE region. In unannealed Z-cut PE-$LiNbO_3$ samples, the PE term source consisted of a plateau of thickness $\delta^Z = 0.65$ μm with a constant H concentration C_H^{Z-0} of 6×10^{21} cm^{-3}. These two quantities yield a total amount of H diffusant $Q_H^{Z-PE} = C_H^{Z-0}\delta^Z = 3.9 \times 10^{17}$ cm^{-2}.

The three parts of Eq. (24) [PE substitutional, PE interstitial, and wv interstitial] are independent and combine to create the total fit to the SIMS profiles. Figure 6 illustrates this procedure for an annealing time of 135 min. This procedure was implemented by use of curve fitting routines found in *Mathematica.*™ Since the interstitial H will diffuse faster than the substitutional H, the interstitial mechanism will be the main contributor deep into the crystal. Near the surface, the substitutional mechanism will be more prevalent. In Fig. 6, the dotted line represents the PE interstitial part, the lower dashed line represents the PE substitutional part, and the dot-dash line represents the contribution due to the wet oxygen. It can be seen that at greater depths, the substitutional part from the PE becomes negligible and the interstitial mechanism (PE plus wv) is almost the only contributor to the H SIMS profile. The solid line in Fig. 6 represents the SIMS profile and the upper dashed line is the sum of the three terms in Eq. (24). Similar

numerical fits were obtained for the H SIMS profiles for the other annealing times and are shown in Fig. 7.

The five coefficients available ($C_{H,s}^{Z-PE}$, $C_{H.i}^{Z-PE}$, $C_{H,i}^{Z-wv}$, D_i^Z, and D_s^Z) to fit the data for an individual time are not unique. Trade-offs can be made between coefficients and still give an excellent fit. Uniqueness for the coefficients is determined when all times are considered using a trial and error process with the following constraints: (1) All of the coefficients should be relatively constant over the different annealing times. The two concentrations, $C_{H,s}^{Z-PE}$ and $C_{H.i}^{Z-PE}$, represent the initial surface concentrations of the PE layer and $C_{H.i}^{Z-wv}$ represents the constant surface concentration due to wet oxygen. (2) The sum of $C_{H,s}^{Z-PE}$ and $C_{H,i}^{Z-PE}$ must equal the initial total PE H surface concentration. The values for these quantities in Z-cut $LiNbO_3$ are summarized in Table III. The values for the diffusivity of Li are included and will be discussed in Part B of this Section.

The best-fit values that were obtained for the diffusivities ($D_s^Z \simeq 5.0 \times 10^{-12}$ cm^2/s and $D_i^Z \simeq 1.4 \times 10^{-11}$ cm^2/s) are nearly constant over the full range of annealing times from 6 to 180 min. Since $D_i^Z \simeq 3D_s^Z$, the larger diffusivity was designated the interstitial H diffusivity D_i^Z and the smaller diffusivity was designated the substitutional H diffusivity D_s^Z. This designation is reasonable because in most materials, the interstitial diffusion coefficient is considerably larger than the substitutional diffusion coefficient.[20] The uncertainties in the various parameters given in Table III for H are: $\pm 2.0 \times 10^{20}$ cm^{-3} for $C_{H,s}^{Z-PE}$, $\pm 2.0 \times 10^{20}$ cm^{-3} for $C_{H,i}^{Z-PE}$, $\pm 0.5 \times 10^{20}$ cm^{-3} for $C_{H,i}^{Z-wv}$, $\pm 0.1 \times 10^{-11}$ cm^2/s for D_i^Z, and $\pm 0.3 \times 10^{-12}$ cm^2/s for D_s^Z.

The amount of H diffusant $Q_H^Z(t)$ present in the Z-cut annealed PE samples after annealing for time t is obtained by integrating Eq. (24) from $x = 0$ to $x = \infty$. There are three contributions to $Q_H^Z(t)$, one from the substitutional H and two

from the interstitial H:

$$Q_H^Z(t) = Q_{H,s}^{Z-PE} + Q_{H,i}^{Z-PE} + C_H^{Z-wv}\sqrt{4D_i^Z t/\pi}\ . \tag{25}$$

Each of these quantities in Eq. (25) is plotted versus $\sqrt{t}$ in Fig. 8 and is labeled separately. The total H diffusant increases with the annealing time according to the SIMS experimental data. The H diffusant due to PE is nearly constant with annealing time, with about 75% in the substitutional component and 25% in the interstitial component. The contribution to $Q_H^Z(t)$ from the water vapor increases with annealing time as $\sqrt{t}$ and adds to the interstitial component. As seen in the figure, the amount of H due to the annealing in a flowing wet oxygen ambient can become quite large and even equal to the amount from proton exchange. However, according to the model presented here, the substitutional H is the most important H component because it forms crystal bonds and alters the extraordinary refractive index.

B. Lithium profiles

The Li depth profiles that were shown in Fig. 1 for the annealed Z-cut PE-$LiNbO_3$ samples were analyzed according to the model presented in Sec. III-B. The Li concentration $C_{Li}^Z(x,t)$ represented in Eq. (18) was used to fit the SIMS measured Li profiles for the Z-cut PE-$LiNbO_3$ samples annealed for 6, 15, 45, and 90 min. The results are shown in Fig. 9. The solid lines are the SIMS measured Li profiles at the designated annealing times and the dashed lines indicate the expression in Eq. (18). With a bulk Li concentration of 1.9×10^{22} cm^{-3}, the values for the Li diffusivity D_{Li}^Z obtained by this procedure were given in Table III. The average Li diffusivity for the different annealing times is $D_{Li}^Z = 4.8 \pm 0.2 \times 10^{-12}$ cm^2/s which is nearly equal to D_s^Z. This equality of diffusivities suggests that the substitutional H diffuses on Li sites during annealing.

C. Refractive index

As described in Sec. II-B, an inverse WKB method[14] was used to determine the $1/e$ depths d_{-1} of the modes for the samples that supported at least three propagating modes. The solid circles in Fig. 10 correspond to the N_e and d_{-1} data given in Table I. The extraordinary refractive index profile given in Eq. (22) may be re-written with Eq. (7) as:

$$n_e^Z(x,t) = n_e^{bulk} + \Delta n_e^{Z-PE} F(x, \delta^Z, D_n^Z t), \tag{26}$$

where n_e^{bulk} is the extraordinary refractive index ($n_e^{bulk} = 2.204$ at $\lambda = 0.6328$ μm) of the unexchanged crystal and D_n^Z is an effective diffusivity of the index. The solid lines in Fig. 10 are the best-fit curves to the experimental data by Eq. (26) and the values used for Δn_e^{Z-PE} and D_n^Z are given in Table IV with D_s^Z for comparison.

Because $D_n^Z \simeq D_s^Z$ and because the same analytical expression fits both the substitutional H profiles and the extraordinary refractive index profiles, a linear relationship should exist between $C_{H,s}^Z(x,t)$ and $[n_e^Z(x,t) - n_e^{bulk}]$. The scaling factor α^Z relating these two quantities is defined by:

$$n_e^Z(x,t) - n_e^{bulk} = \alpha^Z C_{H,s}^Z(x,t). \tag{27}$$

With $D_n^Z \simeq D_s^Z$, this relationship becomes:

$$\Delta n_e^{Z-PE} = \alpha^Z C_{H,s}^{Z-PE}. \tag{28}$$

The values of α^Z determined in this manner are given in Table V. A comparison between the refractive index profiles (solid lines) and the substitutional H profiles (dashed lines) is shown in Fig. 10. Only for $t = 15$ min can a difference in the two curves be observed. Otherwise, the correlation between the refractive index and substitutional H profiles is excellent for times from 45 to 180 min. Based on

this analysis, the average value of α^z is 1.85×10^{-23} (H atoms/cm^3)$^{-1}$ when the value at $t = 15$ min is ignored.

This analysis demonstrates that it is possible to model the depth profile of the extraordinary refractive index in annealed PE-$LiNbO_3$ by use of a single diffusivity. The index profiles are in excellent linear agreement with the substitutional H profiles in Sec. IV-A.

V. ANALYSIS OF DATA FOR X-CUT PE $LiNbO_3$

A. Hydrogen depth profiles

The H depth profiles for the X-cut samples, shown in Fig. 2, were analyzed in the same manner with the following expression for the H concentration:

$$C_H^X(x,t) = C_{H,s}^{X-PE} F(x, \delta^X, D_s^X t) + C_{H,i}^{X-PE} F(x, \delta^X, D_i^X t) + C_H^{X-wv} \mathrm{erfc} \frac{x}{2\sqrt{D_i^X t}}. \tag{29}$$

In unannealed X-cut samples, the PE extended source consisted of a plateau of thickness $\delta^X = 0.75$ μm with a constant H concentration of $C_H^{X-0} = 3.5 \times 10^{21}$ cm^{-3}. These quantities give the total amount of H in the PE layer as $Q_H^{X-PE} = C_H^{X-0}\delta^X = 2.6 \times 10^{17}$ cm^{-2}.

The basic fitting procedure, which was illustrated in Fig. 6 for the H profile in the Z-cut sample annealed for 135 min, was used to fit the X-cut profiles. Numerical fits with the parameters given in Table VI were made to the SIMS measured H profiles for the annealing times of 45, 90 and 240 min, and the results are shown in Fig. 11. The SIMS measured H profiles are the solid lines and the best-fit curves are the dotted lines. The two concentrations, $C_{H,s}^{X-PE}$ and $C_{H,i}^{X-PE}$, represent the initial substitutional and interstitial H surface concentrations in the PE layer. Values for the diffusivities D_s^X and D_i^X, and the water vapor surface concentration C_H^{X-wv} are the other parameters given in Table VI.

The best-fit values that were obtained from the H diffusivities for the X-cut

PE-$LiNbO_3$ crystals are: $D_s^X \simeq 3.4 \times 10^{-12}$ cm^2/s and $D_i^X \simeq 1.3 \times 10^{-11}$ cm^2/s. The diffusivities agree well over the full range of annealing times from 45 to 240 min. While the substitutional H diffusivity is smaller than in Z-cut crystals, the interstitial H diffusivity is nearly equal.

The amount of H diffusant $Q_H^X(t)$ in the X-cut annealed PE samples after annealing for time t is given by:

$$Q_H^X(t) = Q_{H,s}^{X-PE} + Q_{H,i}^{X-PE} + C_H^{X-wv}\sqrt{4D_i^X t/\pi}\ . \tag{30}$$

Each of the quantities in Eq. (30) is plotted versus $\sqrt{t}$ in Fig. 12 and labeled separately. The total H diffusant increases with the annealing time according to the SIMS experimental data. As with Z-cut material, the H diffusant due to proton-exchange is nearly constant with annealing time, with about 75% in the substitutional component and 25% in the interstitial component. Likewise, the contribution from the water vapor increases with annealing time as the $\sqrt{t}$ and forms part of the interstitial component. The amount of H due to the annealing in flowing wet oxygen is equal to the amount from proton-exchange at about 90 min.

An attempt was made to analyze the Li depth profiles for the X-cut samples. However, due to the shallow Li depletion profiles in these samples and the long annealing times, consistent results could not be obtained for the Li diffusivity D_{Li}^X.

B. Refractive index

Values of the propagation coefficients, N_e and d_{-1}, for the X-cut samples listed in Table II, were fitted with Eq. (22) which may be written as:

$$n_e^X(x,t) = n_e^{bulk} + \Delta n_e^{X-PE} F(x, \delta^X, D_n^X t), \tag{31}$$

where D_n^X is the effective index diffusivity for X-cut samples. Very good fits to the data points were achieved for the annealed samples as shown in Fig. 13. The

solid circles correspond to the N_e and d_{-1} data points and the solid curves are the best-fits from Eq. (31). The values used for Δn_e^{X-PE} and D_n^X are given in Table VII with D_s^X for comparison. As with the Z-cut samples, the average value of D_n^X (4.6×10^{-12} cm^2/s) from this analysis is nearly identical to the substitutional H diffusivity D_s^X which was given in Table VI.

Since $D_n^X \simeq D_s^X$, the refractive index change can be linearly related to the substitutional H distribution as:

$$n_e^X(x,t) - n_e^{bulk} = \alpha^X C_{H,s}^X(x,t), \tag{32}$$

where α^X is the scaling factor for the X-cut samples. The values of α^X determined in this manner are given in Table VIII and a comparison of these profiles is shown in Fig. 13. The substitutional H profiles are indicated by the dashed curves and the refractive index profiles are the solid curves. Very good correlation between the refractive index changes and substitutional H profiles exists for annealing times from 45 to 240 min. The average value of α^X based on this analysis is 3.9×10^{-23} (H atoms/cm^3)$^{-1}$.

The analysis for X-cut samples provides further evidence that the extraordinary refractive index profile in annealed PE-$LiNbO_3$ can be modelled by using a single diffusivity and that these profiles are in excellent linear agreement with the substitutional H profiles.

VI. DISCUSSION AND SUMMARY

Our results demonstrate that a significant amount of information can be obtained about the properties of annealed PE-$LiNbO_3$ through a careful diffusion analysis of the SIMS measured H and Li depth profiles. Use of the standard diffusion equation with the appropriate boundary and initial conditions leads to the identification of substitutional and interstitial H, and values for the diffusivities for substitutional H, interstitial H, and Li. Analysis of the total H concentration

provides evidence that wet flowing oxygen is an additional source of interstitial H, as has been shown in other ferroelectric crystals.[21] This procedure has also made it possible to establish a linear correlation between the refractive index change and the substitutional H concentration in the crystal. Previous attempts to correlate H distributions with the refractive index profiles have resulted in non-linear[22] or piece-wise linear[23] relationships. However, since not all of the H measured in the PE-$LiNbO_3$ crystal is optically active, contradictory results have been reported. Furthermore, annealing the crystals in flowing wet oxygen contributes to the H content in the crystal. The additional source of H complicates efforts for finding a valid correlation. Our model is based on a conceptually simple approach which provides a consistent framework that establishes a linear relationship between the refractive index profiles and the substitutional H depth distributions. In addition, the area beneath the refractive index profiles, as represented in Eq. (23), remains nearly constant with annealing. This result agrees with data on similar annealed PE-$LiNbO_3$ planar waveguide layers,[24] and with the values of the substitutional H diffusant as plotted in Figs. 8 and 12.

The scaling factor α that relates the index change to the substitutional H concentration in the crystal depends upon the calibration standard used in the SIMS analysis. In these experiments, a hydrogren (^1H) ion-implanted $LiNbO_3$ sample was used as the calibration standard. Several attempts were made to calibrate with ~~using~~ PE-$LiNbO_3$ samples implanted with deuterium (^2H). For unexplained reasons, spurious profiles of ^2H were obtained and the results could not be used. Moreover, there was a change in the H surface concentration when the same PE-$LiNbO_3$ sample was SIMS analyzed on different days. ~~This may be due to changes in the ambient conditions in the SIMS equipment~~. However, the depth profile curves were of identical shape. When the as-exchanged PE-$LiNbO_3$ samples, and several of the annealed PE-$LiNbO_3$ samples were SIMS analyzed on the same day, the H surface

new p. 22

concentrations for Z-cut and X-cut samples were found to be equal: $C_H^{Z-0} = C_H^{X-0}$. This result means that while the diffusivities determined in Sec. IV and V are not sensitive to the day-to-day SIMS calibration, the absolute values for the H surface concentrations do vary. Recent data obtained from H forward scattering analysis of these samples indicate a larger H concentration in the crystals than that shown in Figs. 1 and 2.[25] Further experiments are needed to clarify this issue.

Assuming that $C_H^{Z-0} \simeq C_H^{X-0}$, the values of α for Z-cut and X-cut samples given in Secs. IV and V need to be adjusted. Using the value for α^Z (1.85×10^{-23} cm^3) as the basis, α^X becomes approximately 2.4×10^{-23} cm^3. The difference in the scaling factor for Z-cut and X-cut crystals is due to the larger index change that was found in the X-cut PE-$LiNbO_3$ samples. It should be noted that while there is some uncertainty in the overall H concentrations and in the values of α, the basic conclusions of this work are unaffected. There are two species of H, substitutional H and interstitial H, and a linear correlation exists between the refractive index change and the substitutional H in annealed PE-$LiNbO_3$.

TABLE I. Effective index values N_e for the observed modes in Z-cut PE-$LiNbO_3$ substrates after annealing at 400°C for time t (min). The $1/e$ depths d_{-1} were determined by an inverse WKB method and are given for samples that supported at least three modes.

	$t = 15$ min		$t = 45$ min		$t = 90$ min		$t = 135$ min		$t = 180$ min	
Mode	N_e	d_{-1}	N_e	d_{-1}	N_e	d_{-1}	N_e	d_{-1}	N_e	d_{-1}
TM_0	2.237	1.0	2.222	1.4	2.216	1.9	2.213	2.3	2.213	2.8
TM_1	2.214	1.7	2.212	2.6	2.209	3.3	2.209	4.1	2.209	4.4
TM_2	2.204	3.1	2.206	4.0	2.206	5.2	2.206	5.8	2.207	6.2
TM_3			2.203	7.0	2.204	7.7	2.205	8.8	2.205	8.9
TM_4									2.204	12.7

TABLE II. Effective index values N_e for the observed modes in X-cut PE-$LiNbO_3$ substrates after annealing at 400°C for time t (min). The $1/e$ depths d_{-1} were determined by an inverse WKB method and are given for samples that supported at least three modes.

	$t = 45$ min		$t = 120$ min		$t = 240$ min	
Mode	N_e	d_{-1}	N_e	d_{-1}	N_e	d_{-1}
TM_0	2.255	0.91	2.233	1.50	2.223	2.17
TM_1	2.232	1.64	2.224	2.68	2.218	3.87
TM_2	2.218	2.58	2.216	3.68	2.215	5.23
TM_3	2.210	4.07	2.212	5.26	2.212	6.96
TM_4	2.208	8.29	2.210	7.87	2.210	9.72

TABLE III. Coefficients for the fit of Eq. (24) to the SIMS measured profiles for H and for the fit of Eq. (18) to the SIMS measured profiles for Li. These parameters are for Z-cut PE-$LiNbO_3$.

Time (mins)	$C_{H,s}^{Z-PE}$ (cm^{-3})	$C_{H,i}^{Z-PE}$ (cm^{-3})	$C_{H,i}^{Z-wv}$ (cm^{-3})	D_s^Z (cm^2/s)	D_i^Z (cm^2/s)	D_{Li}^Z (cm^2/s)
6	4.8×10^{21}	0.8×10^{21}	0.9×10^{21}	5.0×10^{-12}	1.3×10^{-11}	4.8×10^{-12}
15	4.5×10^{21}	1.1×10^{21}	1.0×10^{21}	5.0×10^{-12}	1.5×10^{-11}	5.0×10^{-12}
45	4.2×10^{21}	1.4×10^{21}	0.9×10^{21}	5.0×10^{-12}	1.5×10^{-11}	4.8×10^{-12}
90	4.2×10^{21}	1.4×10^{21}	0.8×10^{21}	5.0×10^{-12}	1.4×10^{-11}	4.8×10^{-12}
135	4.2×10^{21}	1.4×10^{21}	0.9×10^{21}	4.9×10^{-12}	1.4×10^{-11}	
180	4.2×10^{21}	1.4×10^{21}	0.8×10^{21}	5.0×10^{-12}	1.4×10^{-11}	

Table IV. Values of the change of the extraordinary refractive index Δn_e^{Z-PE} together with the diffusivity of the index D_n^Z and the diffusivity of the substitutional H D_s^Z for Z-cut $LiNbO_3$.

Time (min)	Δn_e^{Z-PE}	D_n^Z (cm^2/s)	D_s^Z (cm^2/s)
15	0.100	4.0×10^{-12}	5.0×10^{-12}
45	0.084	5.0×10^{-12}	5.0×10^{-12}
90	0.072	5.0×10^{-12}	5.0×10^{-12}
135	0.072	5.0×10^{-12}	4.9×10^{-12}
180	0.084	5.0×10^{-12}	5.0×10^{-12}

TABLE V. Summary of the extraordinary refractive index change Δn_e^{Z-PE} and the substitutional H concentration $C_{H,s}^{Z-PE}$ which gives the scaling factor α^Z for the Z-cut $LiNbO_3$.

Time (min)	Δn_e^{Z-PE}	$C_{H,s}^{Z-PE}$ (cm^{-3})	α^Z (cm^3)
15	0.100	4.5×10^{21}	2.22×10^{-23}
45	0.084	4.2×10^{21}	2.00×10^{-23}
90	0.072	4.2×10^{21}	1.71×10^{-23}
135	0.072	4.2×10^{21}	1.71×10^{-23}
180	0.084	3.0×10^{21}	2.00×10^{-23}

TABLE VI. Coefficients for the fit of Eq. (29) to the SIMS measured profiles for H. These parameters are for X-cut $LiNbO_3$.

Time (min)	$C_{H,s}^{X-PE}$ (cm^{-3})	$C_{H,i}^{X-PE}$ (cm^{-3})	$C_{H,i}^{X-wv}$ (cm^{-3})	D_s^X (cm^2/s)	D_i^X (cm^2/s)
45	3.0×10^{21}	0.6×10^{21}	0.9×10^{21}	3.4×10^{-12}	1.1×10^{-11}
120	2.8×10^{21}	0.8×10^{21}	0.9×10^{21}	3.4×10^{-12}	1.2×10^{-11}
240	2.8×10^{21}	0.8×10^{21}	0.8×10^{21}	3.5×10^{-12}	1.5×10^{-11}

Table VII. Values of the change of the extraordinary refractive index Δn_e^{X-PE} together with the diffusivity of the index D_n^X and the diffusivity of the substitutional H D_s^X for X-cut $LiNbO_3$.

Time (min)	Δn_e^{X-PE}	D_n^X (cm^2/s)	D_s^X (cm^2/s)
45	0.122	3.3×10^{-12}	3.4×10^{-12}
120	0.110	3.3×10^{-12}	3.4×10^{-12}
240	0.100	3.5×10^{-12}	3.5×10^{-12}

TABLE VIII. Summary of the extraordinary refractive index change Δn_e^{X-PE} and the substitutional H concentration $C_{H,s}^{X-PE}$ which gives the scaling factor α^X.

Time (min)	Δn_e^{X-PE}	$C_{H,s}^{X-PE}$ (cm^{-3})	α^X (cm^3)
45	0.122	3.0×10^{21}	4.07×10^{-23}
120	0.110	2.8×10^{21}	3.99×10^{-23}
240	0.100	2.8×10^{21}	3.57×10^{-23}

References

1. A. Rauber, in *Chemistry and Physics of $LiNbO_3$ Current Topics in Material Science*, edited by E. Kaldis (North Holland, Amsterdam, 1978), Vol. 1, Chap. 7.

2. J. L. Jackel, C. E. Rice, and J. J. Veselka, Appl. Phys. Lett. **41**, 607 (1982).

3. A. Yi-Yan, Appl. Phys. Lett. **42**, 633 (1983).

4. A. Loni, R. M. De La Raue, and J. M. Winfield, Proceedings of the Topical Meeting on Integrated and Guided-Wave Optics, Santa Fe, 1988, OSA, Washington, DC, p. 84-87.

5. R. Richter, T. Bremer, P. Hertel, and E. Krätzig, Phys. Status Solidi A **114**, 765 (1989).

6. A. Loni, R. M. De La Rue, J. M. Zavada, R. G. Wilson, and S. W. Novak, Electron. Lett. **27**, 1245 (1991).

7. J. M. Zavada, H. C. Casey, Jr., C.-H. Chen, and A. Loni, Appl. Phys. Lett. **62**, 2769 (1993).

8. H. C. Casey, Jr., C.-H. Chen, J. M. Zavada, and S. W. Novak, Appl. Phys. Lett. **63**, 718 (1993).

9. W. Bollmann and H. J. Stöhr, Phys. Solidi A **39**, 477 (1977).

10. M. Engelsberg, G. C. do Nascimento, and L. H. Pacobahyba, J. Appl. Phys. **74**, 6427 (1993).

11. S. T. Vohra, A. R. Mickelson, and S. E. Asher, J. Appl. Phys. **66**, 5161 (1989).

12. S. W. Novak, P. Matthews, W. Young, and R. G. Wilson, Proc. 8th Inter. Conf. on Secondary ion Mass Spectrometry (SIMS VIII), edited by A. Benninghoven, K. T. F. Janssen, J. Tümpner, and H. W. Werner (Wiley, Chichester, 1992), p. 471.

13. R. G. Wilson, S. W. Novak, J. M. Zavada, A. Loni, and R. M. De La Rue, J. Appl. Phys. **66**, 6055 (1989).

14. J. M. White and P. F. Heidrich, Appl. Optics **15**, 151 (1976).

15. B. I. Boltaks, *Diffusion in Semiconductors* (Academic Press, New York, 1963) p. 93-128.

16. Ibid., p. 105.

17. U. M. Gosele, private communication.

18. M. De Micheli, J. Botineau, S. Neveu, P. Sibillot, D. B. Ostrowsky, and M. Papuchon, Optics Lett. **8**, 114 (1983).

19. X. F. Cao, R. V. Ramaswamy, and R. Srivastava, J. Lightwave Tech. **LT-10**, 1302 (1992).

20. *Atomic Diffusion in Semiconductors*, edited by D. Shaw (Plenum Press, London, 1973) p. 166, 197.

21. T. W. Simpson and I. V. Mitchell, Nucl. Instrum. Methods B **80-81**, 1178 (1993).

22. C. E. Rice, J. L. Jackel, and W. L. Brown, J. Appl. Phys. **57**, 4437 (1985).

23. M. M. Howerton, W. K. Burns, P. R. Skeath, and A. S. Greenblatt, IEEE J. Quantum Electron. **QE-27** 593, (1991).

24. M. L. Bortz and M. M. Fejer, Opt. Lett. **16**, 1844 (1991).

25. S. Bauman, private communication.

Figure Captions

Fig. 1. The hydrogen and lithium concentration depth profiles in Z-cut PE-$LiNbO_3$ samples, as-exchanged, and after annealing at 400°C for the indicated times. These concentrations were determined by SIMS measurements.

Fig. 2. The hydrogen depth profiles in X-cut PE-$LiNbO_3$ samples, as-exchanged and after annealing at 400°C for the indicated times. These concentrations were determined by SIMS analysis.

Fig. 3. The idealized depth profiles for the hydrogen and lithium concentrations after proton exchange. (a) Hydrogen depth profile with the surface concentration C_H^0 from the surface to the exchange depth δ. (b) Lithium depth profile with the surface concentration C_{Li}^0 to the exchange depth δ and then the constant bulk value C_{Li}^{bulk}.

Fig. 4. Comparison of the fit of the sum of two Gaussians as given by Eq. (5) (dashed curves) with the profiles given by the sum of two error functions as given by Eq. (4). The exchange depth δ was taken as 0.65 μm with one diffusivity taken as 5.0×10^{-12} cm^2/s and the other taken as 1.4×10^{-11} cm^2/s. The diffusion times were taken as $t = 6$ min and $t = 45$ min.

Fig. 5. Attempted fit of a single Gaussian (dashed curve), to the measured diffusion profile (solid curve), for a Z-cut PE-$LiNbO_3$ sample annealed at 400°C for 45 min.

Fig. 6. Best fit of the composite function, as represented by Eq. (24), to the measured H diffusion profile for the Z-cut PE-$LiNbO_3$ samples annealed at 400°C for 135 min. The various quantities plotted in this figure are identified in the inset to the figure.

Fig. 7. Best fit of the composite function, as represented by Eq. (24), to the measured H diffusion profiles for Z-cut PE-$LiNbO_3$ samples annealed at 400°C for the indicated times. The SIMS measured H profiles are given by the solid lines and

the composite functions are indicated by the dotted lines.

Fig. 8. The amount of H diffusant Q_H^Z in Z-cut samples as a function of the square root of the annealing times. The upper dashed curve is the least-squares fit to the total H concentration measured by SIMS for the different annealing times. The lower dashed curve is the fit to the integrated substitutional H concentrations from PE, and the dotted line is the fit to the integrated interstitial H concentrations from PE. The dot-dashed line is the fit to the integrated interstitial H concentrations from the water vapor.

Fig. 9. Fit of the complementary error functions, as represented by Eq. (18), to the SIMS measured Li diffusion profiles for the Z-cut PE-$LiNbO_3$ samples annealed at 400°C for the indicated times. The solid curves represent the SIMS measured Li concentrations and the dashed curves are the best-fit by Eq. (18).

Fig. 10. Comparison of the extraordinary refractive index profiles to the substitutional H concentrations for Z-cut PE $LiNbO_3$ samples annealed at 400°C for times of (a) 15, (b) 45, (c) 90, (d) 135, and (e) 180 min. The solid curves are the Δn_e^Z depth profiles and the dashed curves are the substitutional H profiles. The solid circles represent the extraordinary refractive indices calculated from the prism-coupling measurements.

Fig. 11. Best fit of the composite function, as represented by Eq. (29), to the measured H diffusion profiles for X-cut PE-$LiNbO_3$ samples annealed at 400°C for times of 45, 120, and 240 min. The SIMS measured H profiles are given by the solid lines and the composite functions are indicated by the dotted lines.

Fig. 12. The amount of H diffusant Q_H^X in X-cut samples as a function of the square root of the annealing times. The upper dashed curve is the least-squares fit to the total H concentration measured by SIMS for the different annealing times. The lower dashed curve is the fit to the integrated substitutional H concentration from PE, and the dotted line is the fit to the integrated interstitial H concen-

trations from PE. The dot-dashed line is the fit to the integrated interstitial H concentrations from the water vapor.

Fig. 13. Comparison of the extraordinary refractive index depth profiles to the substitutional H concentrations for X-cut PE $LiNbO_3$ samples annealed at 400°C for times of (a) 45, (b) 120, and (c) 240 min. The solid curves are the Δn_e^X depth profiles and the dashed curves are the substitutional H profiles. The solid circles represent the extraordinary refractive indices calculated from the prism-coupling measurements.

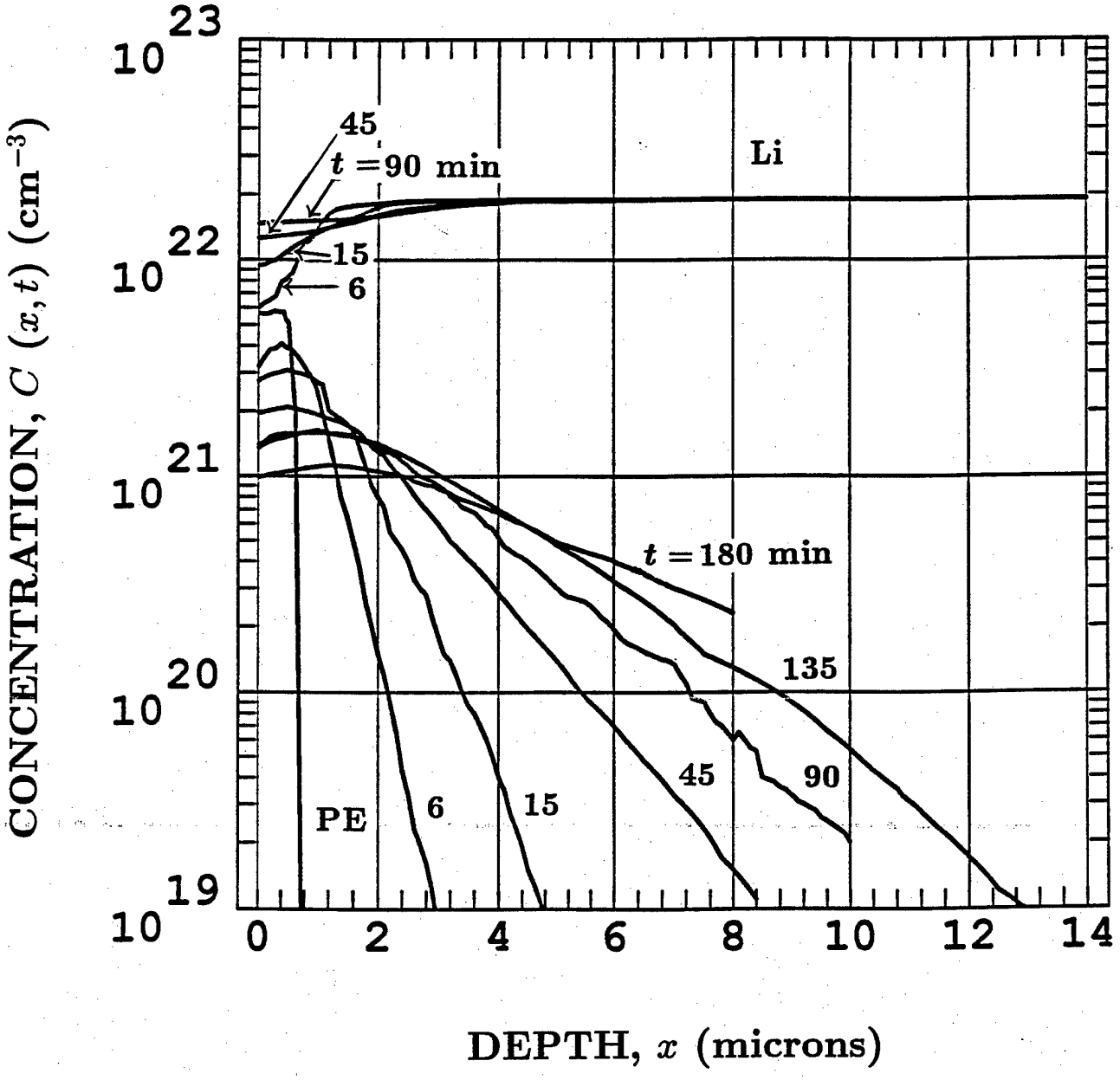
CONCENTRATION, $C\ (x,t)$ (cm^{-3})
10^{23}
10^{22}
10^{21}
10^{20}
10^{19}
45
t = 90 min
Li
15
6
t = 180 min
135
45
90
PE
6
15
0
2
4
6
8
10
12
14
DEPTH, x (microns)

Fig. 1

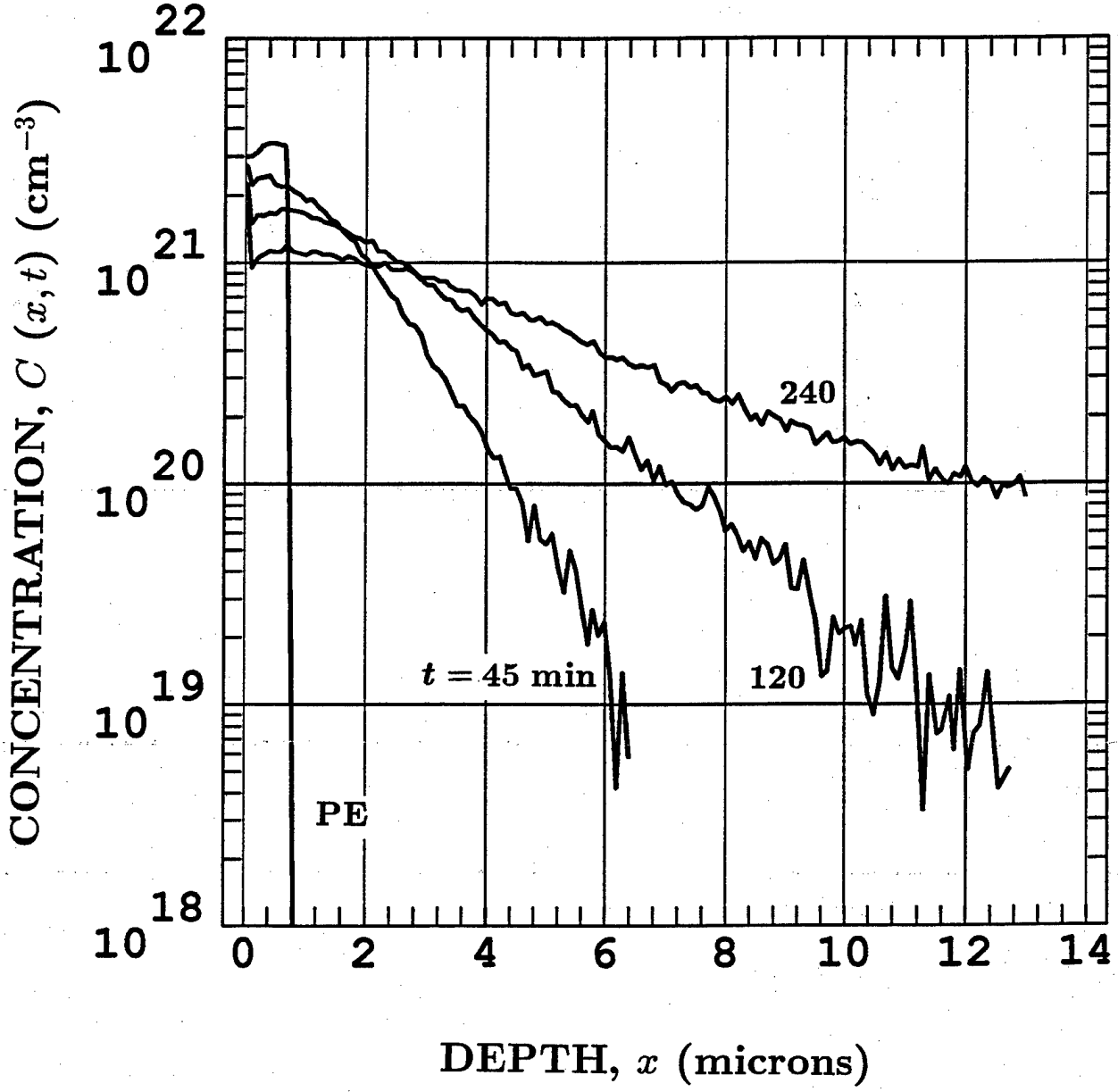
CONCENTRATION, $C\ (x,t)$ (cm^{-3})
10^{22}
10^{21}
10^{20}
10^{19}
10^{18}
0
2
4
6
8
10
12
14
240
120
$t = 45$ min
PE
DEPTH, x (microns)

Fig. 2

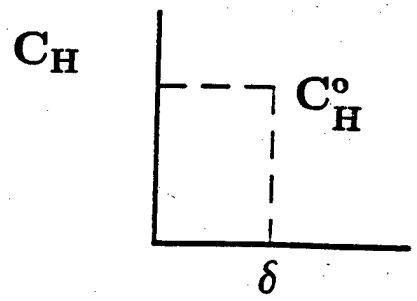

(a)

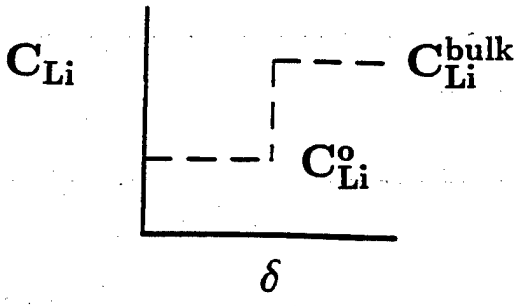

(b)

Fig. 3

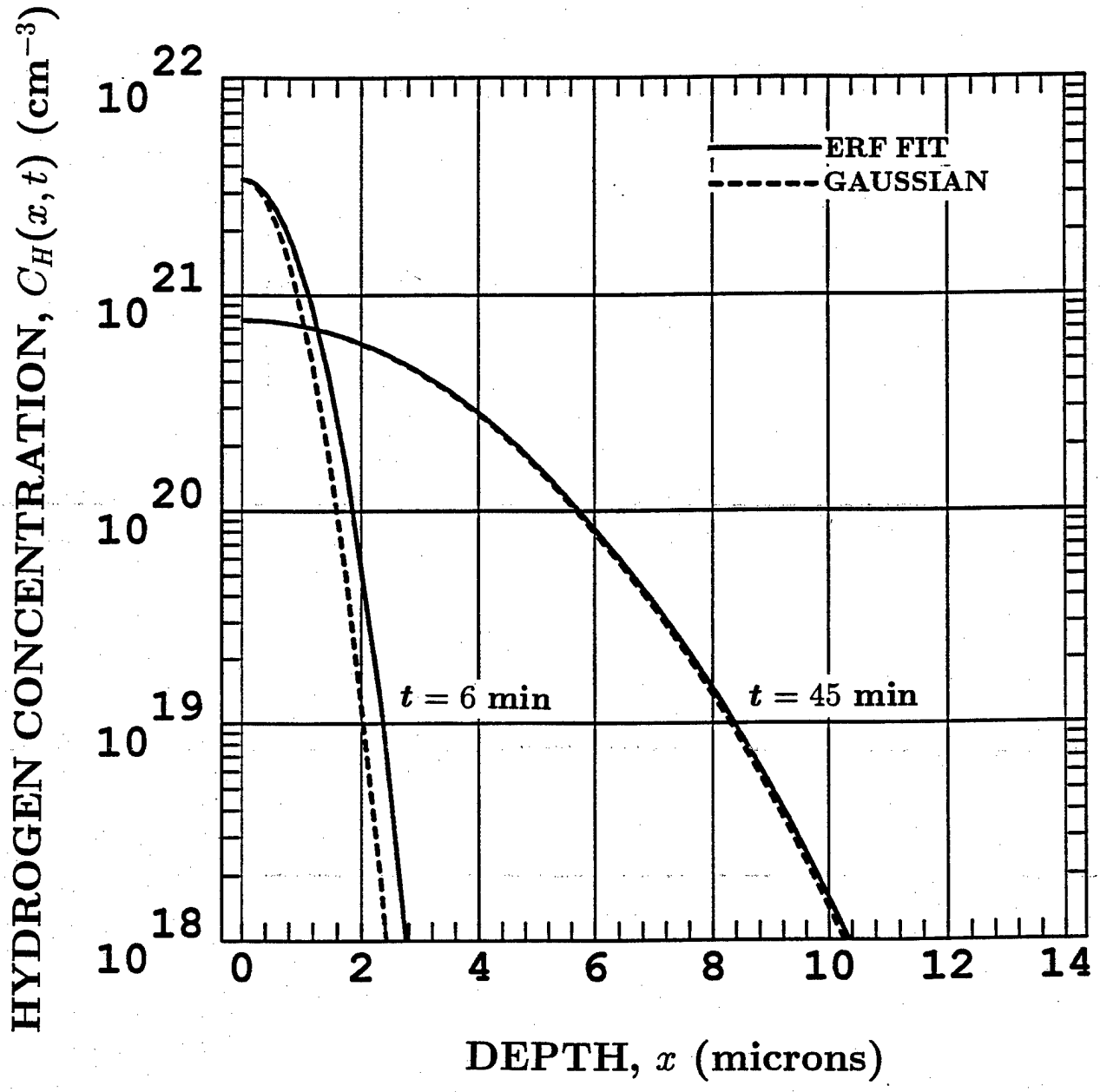
HYDROGEN CONCENTRATION, $C_H(x,t)$ (cm^{-3})
10^{22}
10^{21}
10^{20}
10^{19}
10^{18}
0
2
4
6
8
10
12
14
DEPTH, x (microns)
ERF FIT
GAUSSIAN
$t = 6$ min
$t = 45$ min

Fig. 4

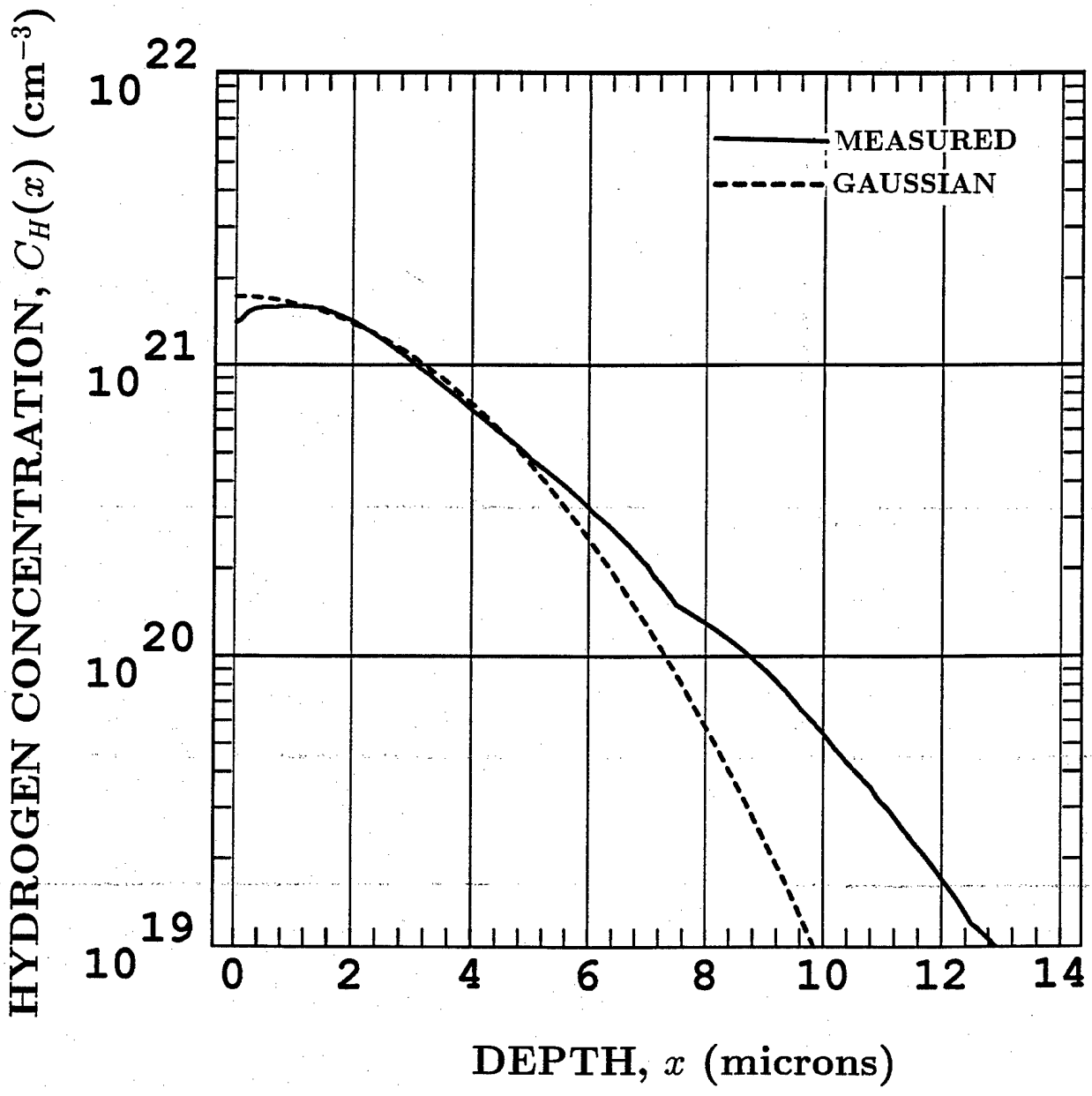
HYDROGEN CONCENTRATION, $C_H(x)$ (cm^{-3})
10^{22}
10^{21}
10^{20}
10^{19}
MEASURED
GAUSSIAN
0
2
4
6
8
10
12
14
DEPTH, x (microns)

Fig. 5

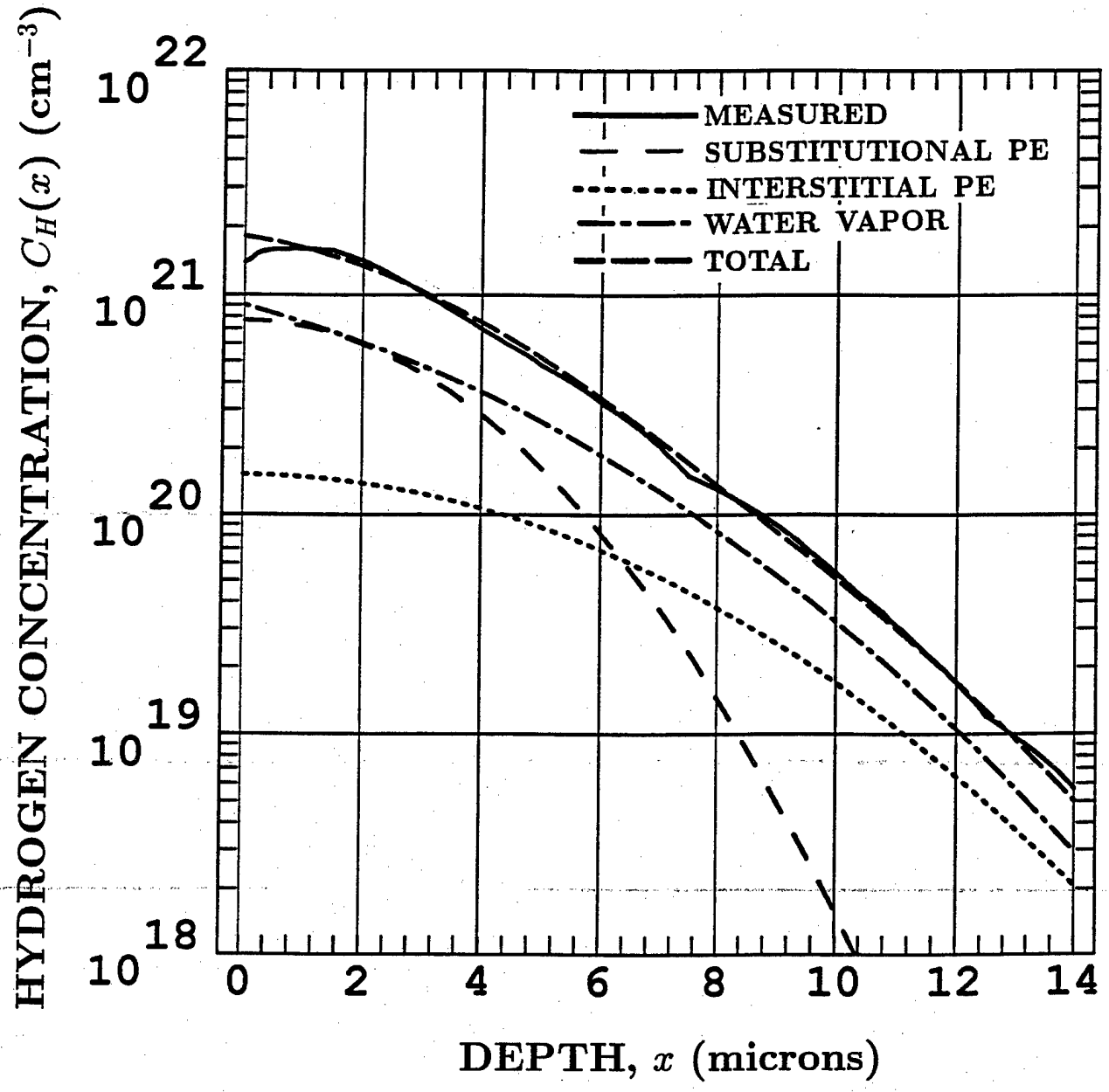
HYDROGEN CONCENTRATION, $C_H(x)$ (cm^{-3})
10^{22}
10^{21}
10^{20}
10^{19}
10^{18}
0
2
4
6
8
10
12
14
DEPTH, x (microns)
MEASURED
SUBSTITUTIONAL PE
INTERSTITIAL PE
WATER VAPOR
TOTAL

Fig. 6

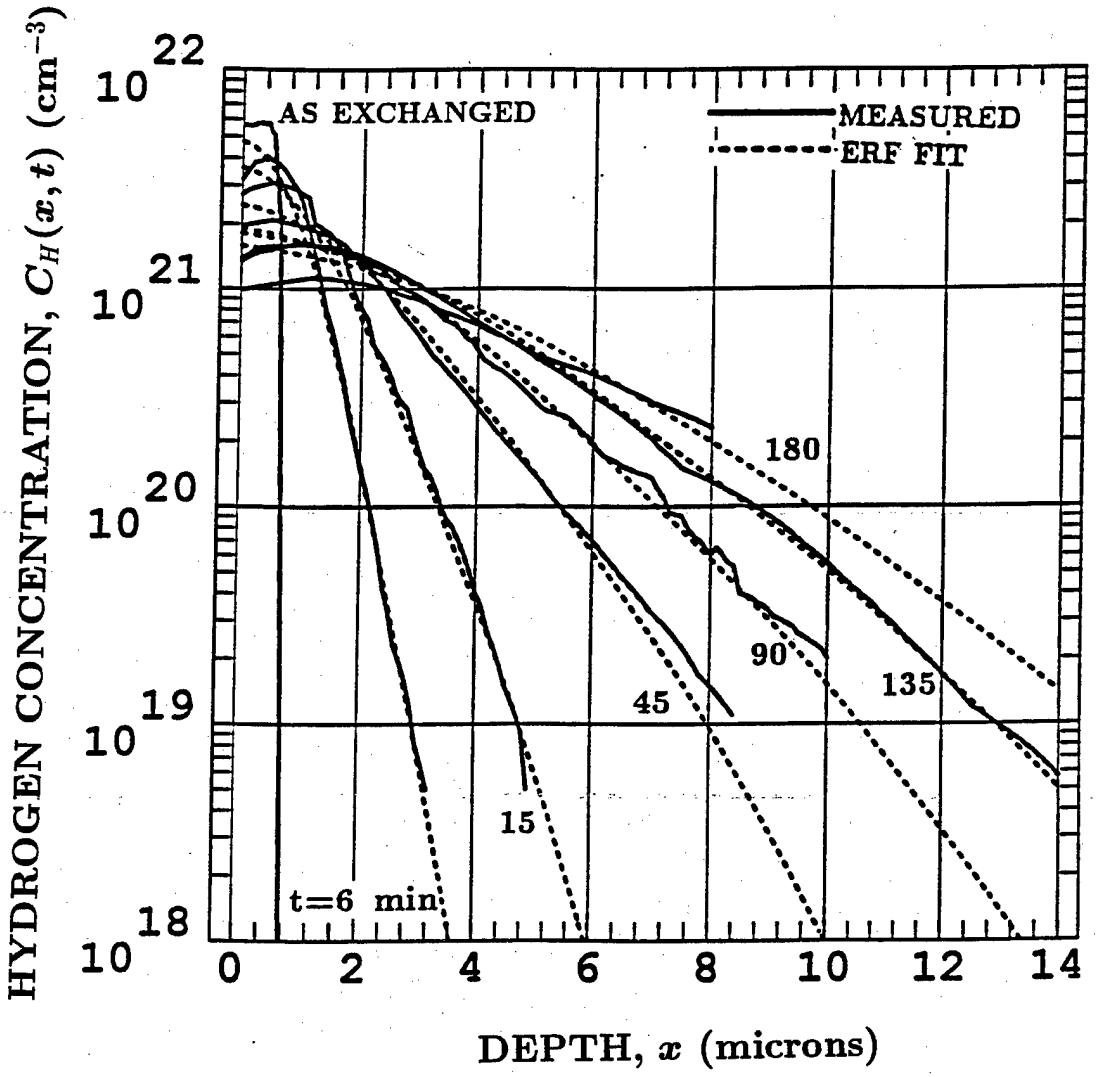
HYDROGEN CONCENTRATION, $C_H(x,t)$ (cm^{-3})
10^{22}
10^{21}
10^{20}
10^{19}
10^{18}
AS EXCHANGED
MEASURED
ERF FIT
180
90
135
45
15
t=6 min
0
2
4
6
8
10
12
14
DEPTH, x (microns)

Fig. 7

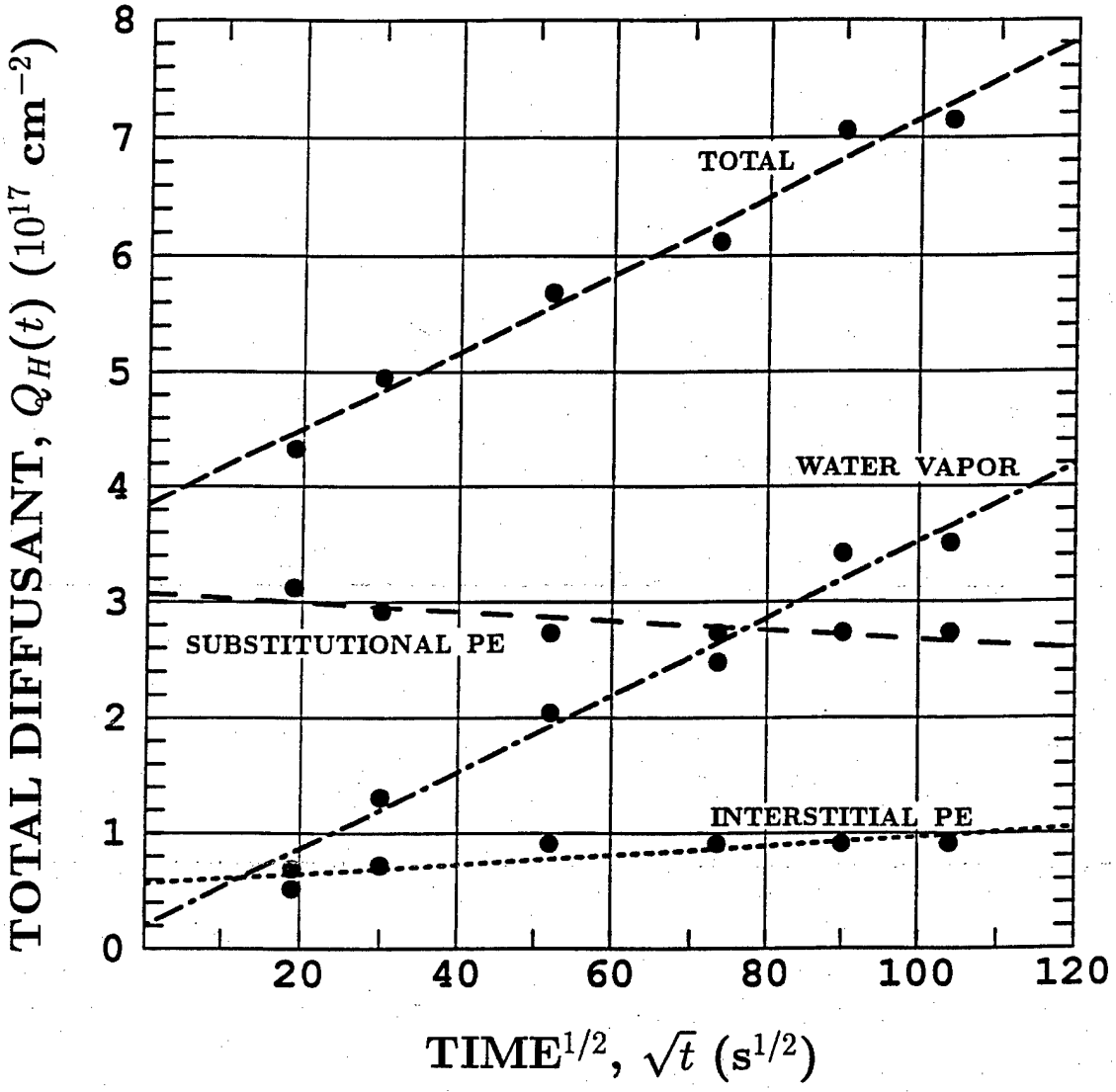
TOTAL DIFFUSANT, $Q_H(t)$ (10^{17} cm^{-2})
TIME$^{1/2}$, $\sqrt{t}$ (s$^{1/2}$)
TOTAL
WATER VAPOR
SUBSTITUTIONAL PE
INTERSTITIAL PE
0
1
2
3
4
5
6
7
8
20
40
60
80
100
120

Fig. 8

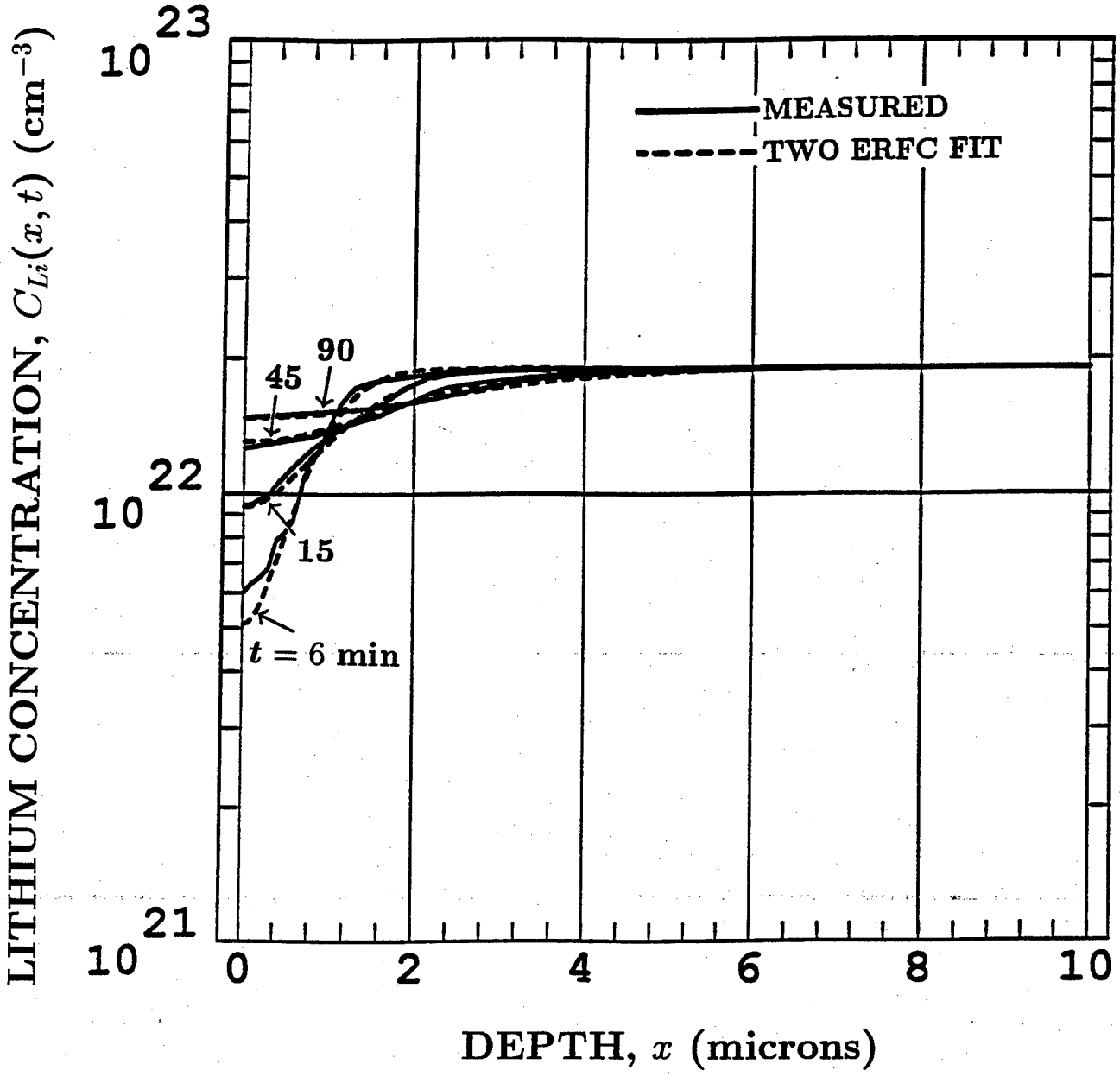
LITHIUM CONCENTRATION, $C_{Li}(x,t)$ (cm^{-3})
10^{23}
10^{22}
10^{21}
MEASURED
TWO ERFC FIT
90
45
15
$t = 6$ min
0
2
4
6
8
10
DEPTH, x (microns)

Fig. 9

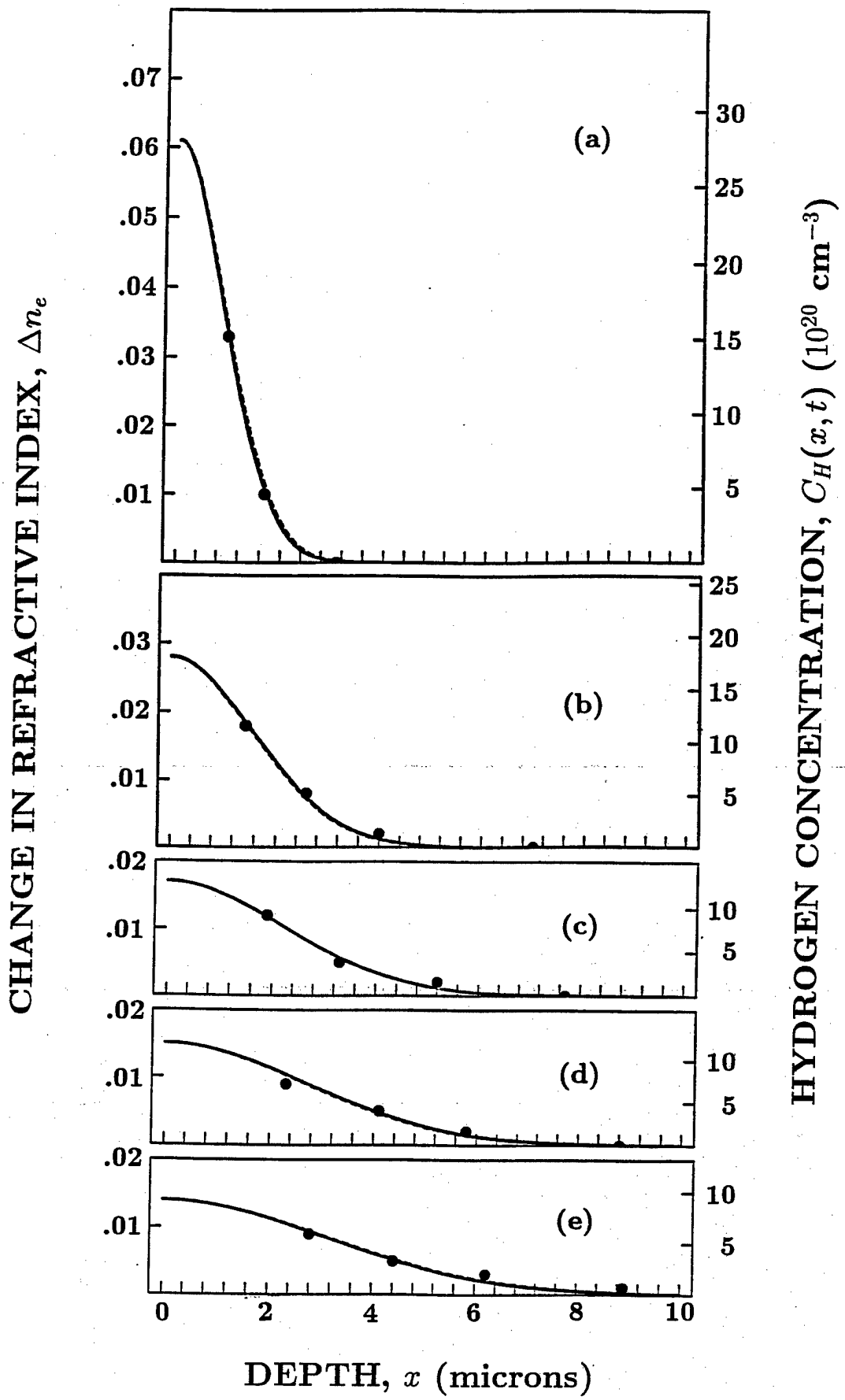
CHANGE IN REFRACTIVE INDEX, Δn_e
HYDROGEN CONCENTRATION, $C_H(x,t)$ $(10^{20}$ cm$^{-3})$
DEPTH, x (microns)
(a)
(b)
(c)
(d)
(e)
.07
.06
.05
.04
.03
.02
.01
30
25
20
15
10
5
0
2
4
6
8
10

Fig. 10

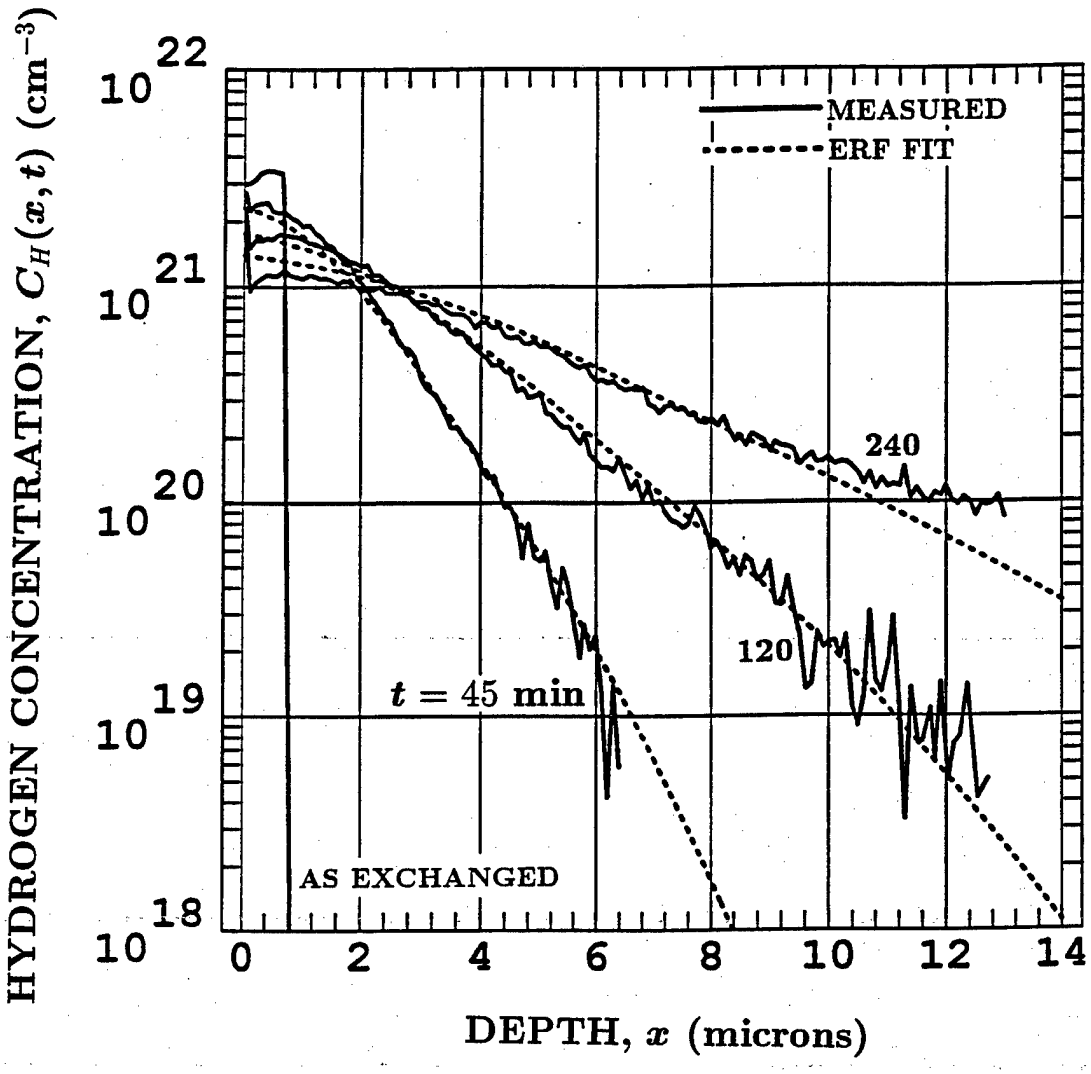
HYDROGEN CONCENTRATION, $C_H(x,t)$ (cm^{-3})
10^{22}
10^{21}
10^{20}
10^{19}
10^{18}
MEASURED
ERF FIT
240
120
$t = 45$ min
AS EXCHANGED
0
2
4
6
8
10
12
14
DEPTH, x (microns)

Fig. 11

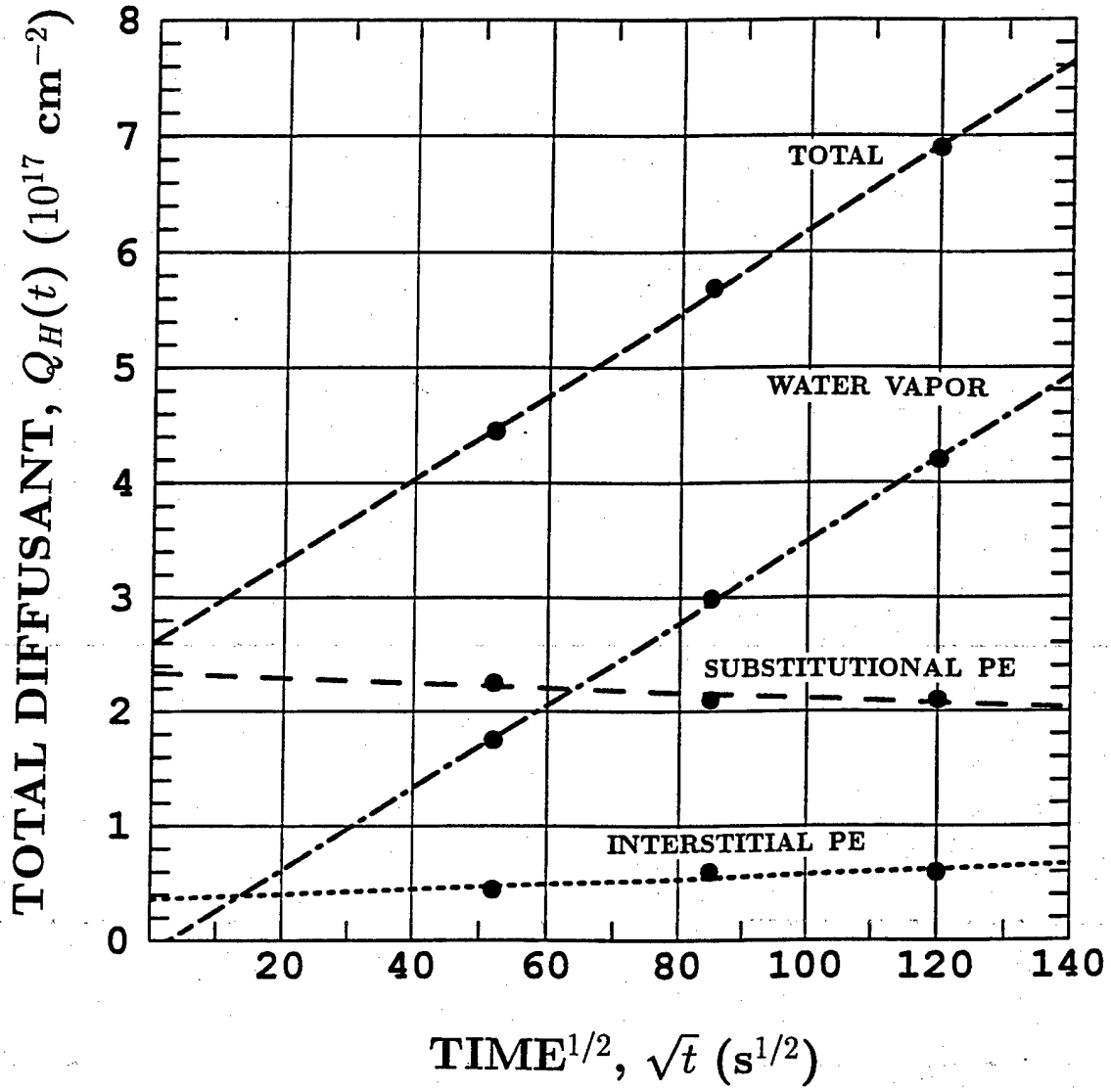
TOTAL DIFFUSANT, $Q_H(t)$ $(10^{17}$ cm$^{-2})$
TIME$^{1/2}$, $\sqrt{t}$ (s$^{1/2}$)
TOTAL
WATER VAPOR
SUBSTITUTIONAL PE
INTERSTITIAL PE
0
1
2
3
4
5
6
7
8
20
40
60
80
100
120
140

Fig. 12

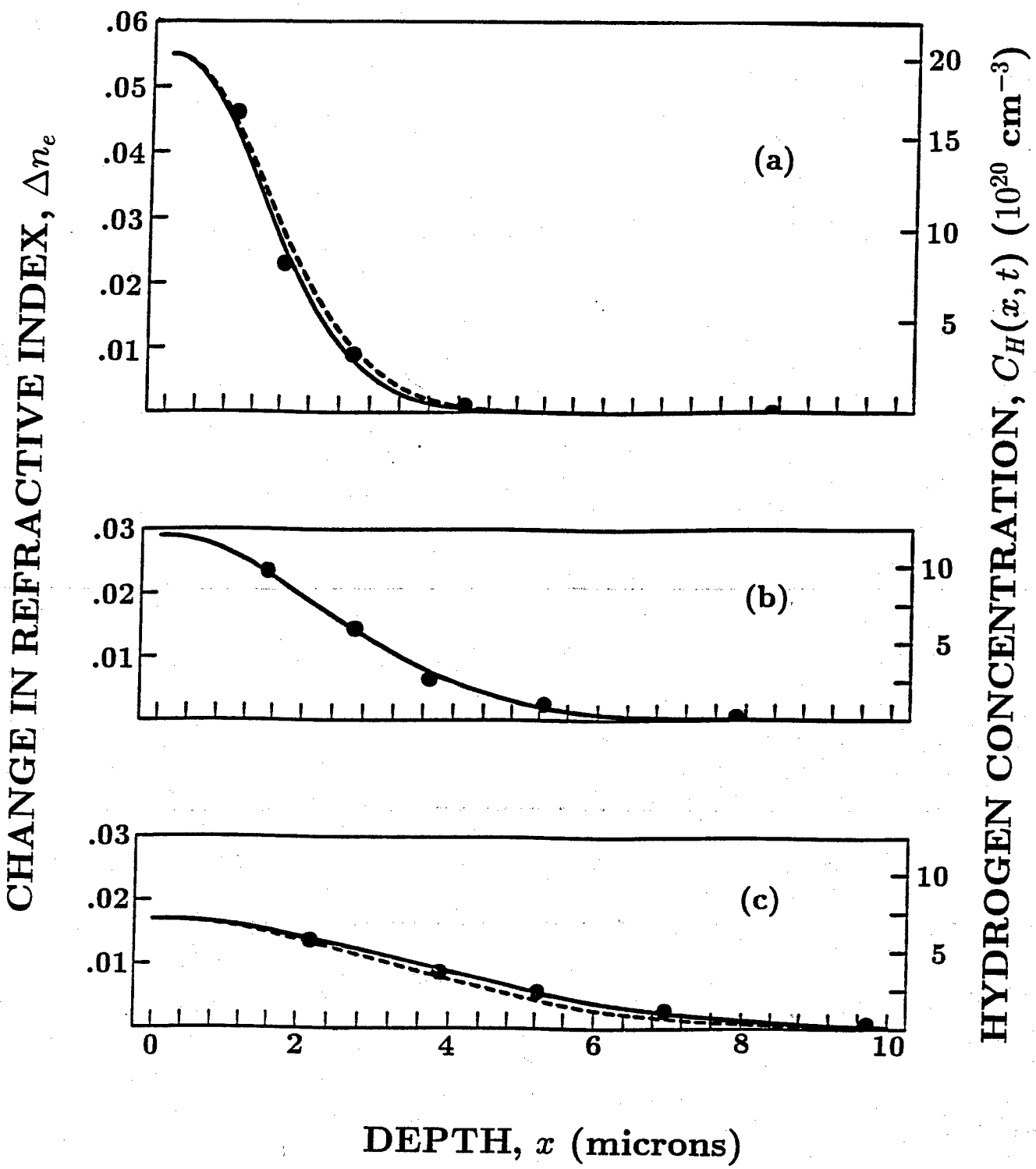
CHANGE IN REFRACTIVE INDEX, Δn_e
.06
.05
.04
.03
.02
.01
(a)
20
15
10
5
.03
.02
.01
(b)
10
5
.03
.02
.01
(c)
10
5
0
2
4
6
8
10
DEPTH, x (microns)
HYDROGEN CONCENTRATION, $C_H(x,t)$ $(10^{20}$ cm$^{-3})$

Fig. 13